ARTICLES

Geochronology of Bimodal Alkaline Volcanism in the Balcones Igneous Province, Texas: Implications for Cretaceous Intraplate Magmatism in the Northern Gulf of Mexico Magmatic Zone

William R. Griffin, Kenneth A. Foland,[1] *Robert J. Stern, and Matthew I. Leybourne*[2]

Department of Geosciences, University of Texas at Dallas, P.O. Box 830688, MS FO21, Richardson, Texas 75083, U.S.A.
(e-mail: griffin@utdallas.edu)

ABSTRACT

Small-volume Late Cretaceous monogenetic alkaline volcanism along the southern margin of North America resulted in a broad igneous belt more than 1200 km long from the Trans Pecos region of west Texas to central Mississippi, collectively forming a northern Gulf of Mexico magmatic zone (NGMMZ). The locus of igneous activity is associated with the discontinuity separating Mesoproterozoic cratonic lithosphere and Jurassic transitional lithosphere, a zone approximating the southern margin of Laurentia, the subsurface trend of the Pennsylvanian Ouachita orogenic belt, and the trace of the Miocene Balcones fault zone in Texas. Although previous studies have attempted to determine the ages of igneous activity in the region, few well-constrained geochronologic data using modern high-resolution techniques are available. We determined the age of eruption for the Balcones igneous province (BIP), a 400-km-long subsegment of the NGMMZ, using modern $^{40}Ar/^{39}Ar$ and U-Pb geochronology methods. Our results suggest that previously reported $^{40}K/^{40}Ar$ and $^{40}Ar/^{39}Ar$ ages underestimate the age of igneous activity by as much as 17%. New ages from this study, along with reevaluation of previous results, suggest that BIP igneous activity occurred in two discrete phases, each lasting only 2.6 m.yr. and separated by 2.7 m.yr.: older mafic volcanism occurred between 81.5 and 84.1 Ma and younger felsic volcanism between 76.2 and 78.8 Ma. The total interval of 8 m.yr. for BIP igneous activity is much shorter than had previously been inferred. The best geochronologic results are obtained from U-Pb dating of zircon mineral (phonolites) separates and $^{40}Ar/^{39}Ar$ dating of phlogopite (nephelinites and basanites) and amphibole (phonolites) separates.

Online enhancements: appendix tables.

Introduction

The southern margin of North America experienced widespread alkaline magmatism during Late Cretaceous time, ranging from west Texas to central Mississippi, collectively forming a northern Gulf of Mexico magmatic zone (NGMMZ; fig. 1; e.g., Byerly 1991). The timing and duration of this activity are poorly understood because of a lack of modern high-resolution geochronologic data (Baksi 1997). The magmatism is constrained to have occurred between 108 ± 5 Ma (Prairie Creek complex, AR; Zartman 1977) and 66 ± 5 Ma (Jackson Dome, MS; Merrill 1983). It is important to understand the temporal history of a magmatic field because time-space relationships provide testable criteria to distinguish between various magmatic models (i.e., mantle plumes, edge convection, lithospheric delamination). Zartman (1977) recognized that alkaline rocks are commonly emplaced after cessation of orogeny or in anorogenic settings and that tectonic setting is often poorly understood in the genesis of alkaline rock suites, contending that accurate dating is essential for understanding their

Manuscript received July 18, 2008; accepted August 1, 2009.

[1] Department of Geological Sciences, Ohio State University, 275 Mendenhall Lab, 125 South Oval Mall, Columbus, Ohio 43210, U.S.A.

[2] Ocean Exploration, GNS Science, Box 30-368, Lower Hutt 5040, New Zealand.

[The Journal of Geology, 2010, volume 118, p. 1–21] 0022-1376/2010/11801-0001$15.00. DOI: 10.1086/648532

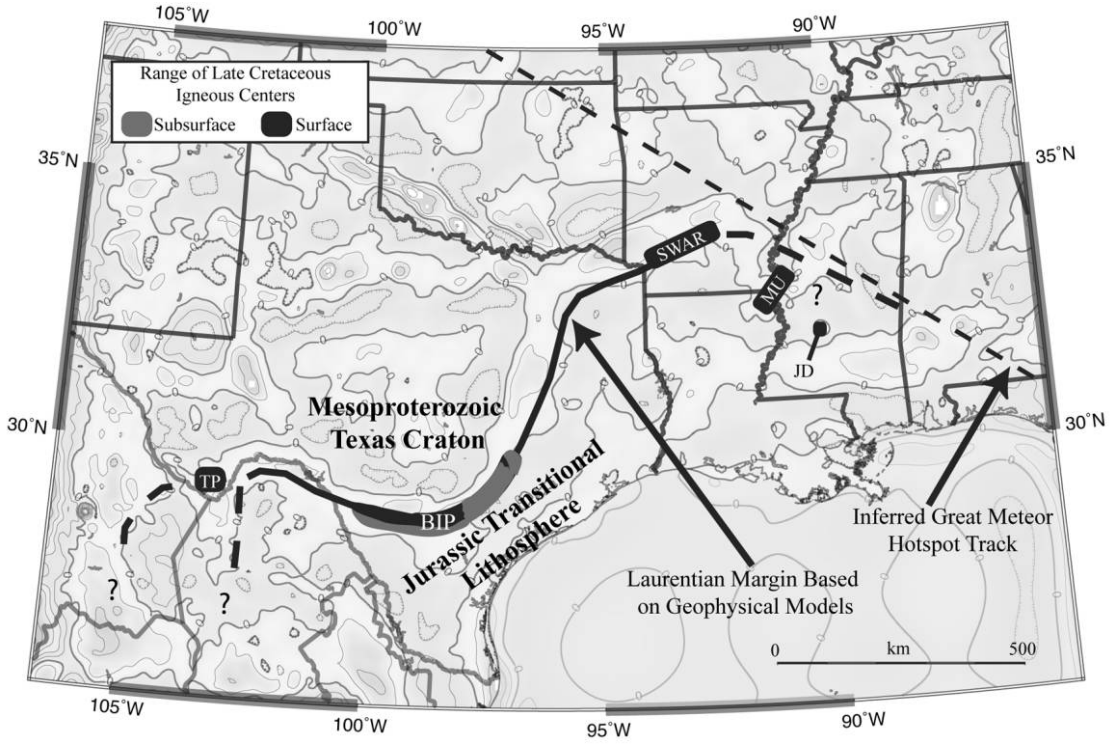

Figure 1. Filtered (40–250-km wavelengths passed) gravity map of the southern margin of North America (after G. R. Keller, pers. comm., 2008). The Laurentian margin defines the discontinuity between Mesoproterozoic Texas cratonic lithosphere and Jurassic transitional lithosphere. Segments of the larger northern Gulf of Mexico magmatic zone are labeled as follows: *TP* = Trans Pecos, *BIP* = Balcones igneous province, *SWAR* = southwest Arkansas, *MU* = Monroe uplift, and *JD* = Jackson Dome. The thick dashed lines represent possible extensions of the Laurentian margin; the thin dashed line represents the inferred track of the Great Meteor hot spot (after Duncan 1984).

origins. This is certainly true for the NGMMZ, where a mantle plume origin has been suggested (Cox and Van Arsdale 2002) and magmatism is predicted to have migrated along a hot spot track from W to E through the region. A review of the literature shows that alkaline volcanic complexes are variable with respect to the duration of activity in individual complexes, ranging from short-lived monogenetic fields that complete their entire eruptive cycles over a few decades or less to long-lived polygenetic fields with repeated eruptive cycles over 10 s to >100 m.yr. (Nielsen 1981; Fitton 1987; Barker 1996; Edwards and Russell 1999, 2000; Ngounouno et al. 2000; Ulrych et al. 2000; Yongtao and Anchun 2003; Gourgaud and Vincent 2004; Bailey and Woolley 2005; Cook et al. 2005; Johansen et al. 2005; Liégeois et al. 2005). Testing models for the tectonic setting of alkalic provinces requires precise and accurate geochronology data.

This study focuses on the geochronology of Late Cretaceous alkaline magmatism in the Balcones igneous province (BIP) of Texas (fig. 2). This is a 400-km-long, 100-km-wide subsegment of the larger NGMMZ. New $^{40}Ar/^{39}Ar$ and U-Pb results from BIP mineral separates are presented, evaluated, and integrated with results from previous studies to more tightly constrain the timing and duration of BIP magmatic activity. BIP magmatism resulted in >200 (Ewing and Caren 1982) intrusive and eruptive centers along the reactivated discontinuity between Grenville-age (1.1–1.3-Ga) Texas craton and Jurassic (~160–180-Ma) transitional lithosphere of the northern margin of the Gulf of Mexico basin. This discontinuity is also approximated by the subsurface trend of the Pennsylvanian (~300-Ma) Ouachita orogenic belt and the Miocene-age (25–10-Ma) Balcones fault zone (Galloway et al. 1991) in south central Texas (fig. 2). Low-degree partial melts from the focal zone (FOZO) and the FOZO + high-μ (HIMU) asthenospheric sources in the upper mantle produced a suite of monogenetic volcanic rocks in compositional range of melilite olivine nephelinites, olivine nephelinites, nepheline basanites, alkali basalts, phonotephrites, tephriphonolites, and

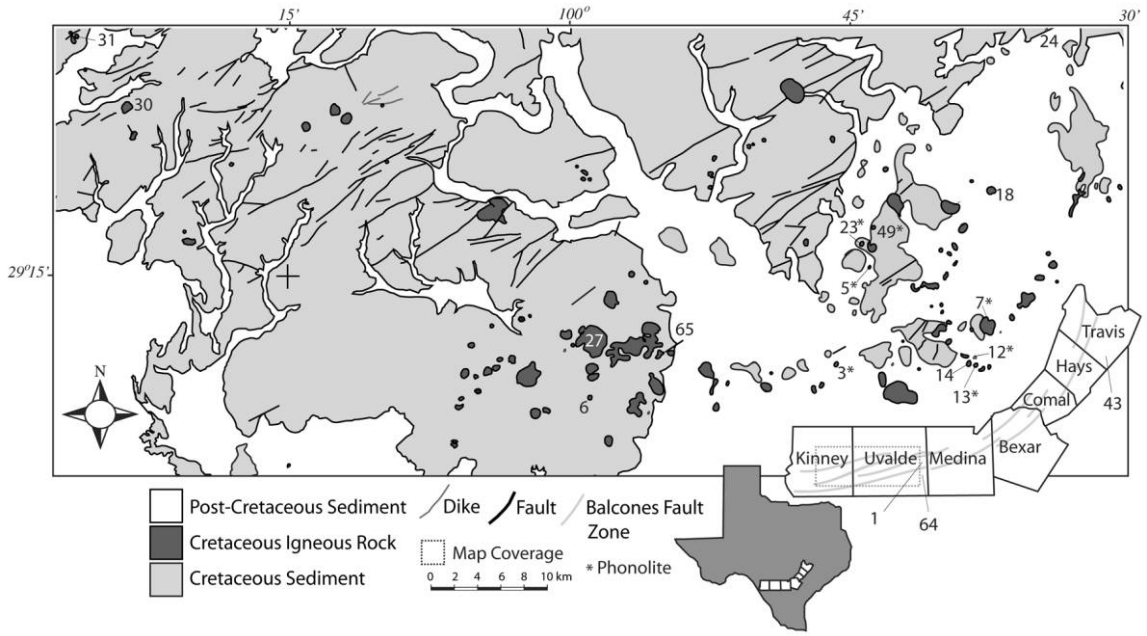

Figure 2. Map of the Balcones igneous province (after Griffin 2008). Numbered locations correspond to sample locations where ages were derived, as detailed in table 3. Phonolitic outcrops are indicated by an asterisk next to the location number.

phonolites (Griffin 2008; Griffin et al. 2009). On the basis of the major, trace, and radiogenic isotope compositions of BIP igneous rocks, we have suggested that the location and style of magmatism in the BIP were intimately linked to an important lithospheric discontinuity (Griffin 2008; Griffin et al. 2009); however, the temporal aspects are less clear because of the paucity of modern, high-resolution geochronological data. Previous studies of the BIP used $^{40}K/^{40}Ar$ techniques to date a number of volcanic centers (Burke et al. 1969; Baldwin and Adams 1971), but only a few ages using higher-precision $^{40}Ar/^{39}Ar$ techniques are available (Miggins et al. 2004), and no U-Pb zircon ages are reported. Although the BIP can be seen in the field to consist of many low-volume, monogenetic volcanoes and plugs, existing radiometric ages suggest protracted activity from 100–66 Ma, on the basis of the stratigraphic relationships of pyroclastic deposits and fossiliferous sediments (Barker 1996), to as short as 82–72 Ma, on the basis of $^{40}Ar/^{39}Ar$ geochronology (Miggins et al. 2004).

Stratigraphic relations are difficult to determine at most BIP volcanic centers because of poor exposure. The stratigraphically best-studied outcrop is Pilot Knob, at the northeastern extreme of the BIP (fig. 2, *43*; Strong 1957; Barker and Young 1979; Ewing and Caren 1982; Young et al. 1982), and it was isotopically dated by Baldwin and Adams (1971). Tuff associated with the outcrop was found to interfinger with Upper Dessau (Upper Austin group, Upper Santonian) strata. The Santonian stage is constrained between 83.5 ± 0.7 and 85.8 ± 0.7 Ma (Gradstein et al. 2005). Fracturing of Dessau strata near Pilot Knob was interpreted by Strong (1957) as evidence for the timing of volcanism, giving a somewhat older age than the average $^{40}K/^{40}Ar$ whole-rock age of 79.5 ± 3 Ma (Baldwin and Adams 1971). Young et al. (1982) contended that the earliest magmatism at Pilot Knob was contemporaneous with the middle Dessau Formation, and they discussed areas proximal to the center that were coeval with the boundary between the Austin and Taylor groups.

Stratigraphic relationships elsewhere in the BIP are less clear than at Pilot Knob. In a literature review of the BIP, Matthews (1986) concluded that magmatism occurred between the Coniacian and the Campanian stages (Austin and Taylor groups) and separated the province into three segments on the basis of variations of the apparent stratigraphic ages. The northern segment included centers in the eastern extreme of the BIP (including Pilot Knob), centered on Travis County (fig. 2). Magmatism there was contemporaneous with Santonian to Campanian strata (Austin and Taylor groups; Mat-

thews 1986); this corresponds to an absolute age range of 89.3 ± 1 to 70.6 ± 0.6 Ma (Gradstein et al. 2005). The central segment, southeast of Bexar County (fig. 2), contains no exposures of igneous rock, but subsurface centers have been cut by drilling interpreted to be contemporaneous with Coniacian to Santonian strata of the Austin Group (89.3 ± 1 to 83.5 ± 0.7 Ma; Gradstein et al. 2005), stratigraphically older than the igneous centers in the northern subprovince (Matthews 1986). The southern segment is the locus of the most intense magmatism, as indicated by the highest-concentration BIP volcanoes and plugs, and is centered on Uvalde County (fig. 2). Matthews (1986) concluded that magmatism in the southern segment was stratigraphically younger than that in the central and northern segments, contemporaneous with Santonian and Campanian strata (Austin and Taylor groups) to Maastrichtian strata (Escondido Formation), corresponding to an age range of 89.3 ± 1 to 65.5 ± 0.3 Ma (Gradstein et al. 2005). Our experience in the field was that the stratigraphic relations of volcanic horizons, as well as intrusive relationships, were difficult to observe because of poor exposure, so we argue that the best method of further defining the age and duration of magmatism in the BIP is by isotopic methods.

This study provides new constraints on the age of the BIP by reporting results of $^{40}Ar/^{39}Ar$ and U-Pb analyses of high-purity amphibole, phlogopite, and zircon mineral separates. These data are used to address the following questions: (1) Which minerals and techniques provide the most reliable ages of BIP igneous activity? (2) What was the timing and duration of BIP magmatism? (3) Were the various BIP lithologies comagmatic or confined within discrete time intervals? Answers to these questions can provide general insights regarding the differences between monogenetic and polygenetic magmatism and the factors influencing the duration of activity in the region.

Geologic Background

The geological history of the BIP region is related to tectonic events associated with the tectonic evolution of the southern margin of North America. This includes accretion of Mesoproterozoic (1.3-Ga) lithosphere resulting from the Grenville orogeny, followed by the accretion of Pennsylvanian-age (320–300-Ma) lithosphere associated with the Ouachita orogeny (Galloway et al. 1991) and the opening of the Gulf of Mexico in Early Mesozoic time (~200–160 Ma). The opening of the Gulf of Mexico began by rifting, attenuating the Ouachita lithosphere, and it culminated in seafloor spreading during mid-Jurassic time (~160 Ma), about 80 m.yr. before the onset of BIP magmatism (Sawyer et al. 1991). The discontinuity between the cratonic lithosphere of North America and attenuated transitional lithosphere on the NW flank of the Gulf of Mexico oceanic basin localized the Late Cretaceous BIP magmatism (Griffin 2008; Griffin et al. 2009). The location of the BIP along this discontinuity is consistent with a number of different magmatic mechanisms explored by Griffin (2008), including edge convection (King and Anderson 1998), lithospheric delamination (i.e., Kay and Kay 1993), and lithospheric rifting (Corti et al. 2003). Although strongly alkaline, silica-undersaturated intraplate melts, such as those of the BIP, are commonly associated with continental rifting (i.e., Mitchell and Platt 1983). Griffin (2008) concluded that no major rifting events occurred in the region during Late Cretaceous time. Instead, stress regimes imposed on the region (Bird 2002) were sufficient to create small degrees of extension perpendicular to the lithospheric discontinuity, allowing low-degree decompression melting of volatile-enriched upper mantle sources with FOZO and HIMU affinities. BIP igneous activity includes shallow marine eruptions of nephelinites and basanites, as well as shallow intrusions of phonolite. The discontinuity was reactivated as late as Miocene time (25–10 Ma), forming the Balcones escarpment (Galloway et al. 1991); however, the reactivation occurred long after BIP igneous activity ended.

Methods

Approximately 45 kg of bulk rock was collected at each sampling location. All samples were prepared at the University of Texas at Dallas Department of Geoscience sample preparation lab by removing weathered surfaces with a rock saw, crushing them a steel-jaw crusher, washing and drying the rock chips, and powdering them in a Bico disk mill pulverizer to pass through a 60-mesh sieve, followed by an 80-mesh sieve. Powder splits between 60–80 and 80–100 mesh were preserved for zircon (felsic rocks), amphibole, and nepheline-K-feldspar concentrate (felsic rocks) and phlogopite (mafic rocks) separation.

Ten samples were processed for zircon extraction (one melilite olivine nephelinite, two olivine nephelinites, one phonotephrite, and six phonolites). The sieved material for zircon separation was concentrated for heavy minerals on a shaker table,

dried, and passed through a Frantz isodynamic separator. The 1.6-A (maximum) nonmagnetic split was subjected to heavy-liquid separation in methylene iodine and handpicked under a binocular microscope. Zircon in the mafic rocks is very rare to nonexistent, with one sample yielding a single crystal that produced an age (although the degree of uncertainty was high) consistent with that of phlogopite separates recovered from other mafic samples in the area. Other zircons from mafic samples yielded much older (xenocrystic) ages or were discordant; these nevertheless provide information about BIP basement. Zircon abundance in the phonotephrite and phonolites ranges from abundant to nonexistent. One sample yielded a large population, two yielded moderate populations, two yielded small populations, and one yielded no zircon. As was found in the mafic samples, the felsic rocks carry rare zircons yielding much older (xenocrystic) ages, although compared with the mafic rocks, those make up a smaller proportion of the total populations recovered. Future work aimed at recovering zircon from the BIP should concentrate the effort on the felsic rocks only because the results obtained from mafic zircons were not useful in determining the age of eruption and cooling for individual outcrops. Baddeleyite separation was not attempted but should be in future studies.

Nine mafic and 11 felsic samples were processed for $^{40}Ar/^{39}Ar$ mineral separation. Crushed splits for phlogopite, amphibole, and nepheline-K-feldspar concentrate separation were washed to remove fines, dried, and passed through a Frantz isodynamic separator; magnetic splits 0.3–0.4 and 0.4–0.5 A were targeted for phlogopite and amphibole, respectively. Further concentration was achieved by heavy-liquid separation in Bromoform and handpicking under a binocular microscope. Phlogopite was targeted in the mafic rocks, even though rare in most samples, because no other suitable mineral targets exist for $^{40}Ar/^{39}Ar$ geochronology. Amphibole was targeted for separation in the felsic rocks because it is the most common suitable mineral for $^{40}Ar/^{39}Ar$ analyses. Nepheline-K-feldspar concentrates were recovered from the 1.6-A nonmagnetic Frantz split. Future work requiring mica separates should focus on the mafic rocks, and work requiring amphibole separates should focus on the felsic rocks of the BIP.

Zircons were analyzed at the USGS sensitive high-resolution ion microprobe reverse geometry (SHRIMP-RG) instrument housed at the Stanford University Microanalysis Center (SUMAC). Zircons were mounted on glass slides, using double-sided tape, in 1 × 6-mm rows. The grains were cast into 25 × 4-mm epoxy disks and polished to 1-μm finish. Transmitted light images were made on an optical microscope to reveal the surface textures of the grains. The grain mount disk was then Au-coated by standard sputter-coating techniques, and cathode luminescence (CL) images (fig. 3) were made using a JEOL 5600LLV scanning electron microscope to reveal the interior zonation of each grain. The grain mounts were then washed in a saturated EDTA solution, dried, and gold-coated for introduction to the SHRIMP-RG.

Analyses of individual zircons began by rastering a primary O^{2-} ion beam at an intensity of 4–6 nA for 120 s to remove the Au coat and surface contamination from the analytical spot. The primary ion beam was focused to approximately 20–40 μm and rastered over the analytical spot for 12 min to produce secondary ions from an ablation spot approximately 1–2 μm deep. Peaks for $^{90}Zr_2^{16}O$, ^{204}Pb, background (0.050 amu above ^{204}Pb), ^{206}Pb, ^{207}Pb, ^{208}Pb, ^{238}U, $^{232}Th^{16}O$, and $^{234}U^{16}O$ were sequentially measured. An autocentering procedure performed on guide peaks of variable or low abundance (i.e., $^{90}Zr_2^{16}O$ at 0.165 amu below the ^{204}Pb peak) improved peak center location reliability and eliminated isobaric interferences.

Data were processed off-line at the end of each analytical session, using SQUID 1.02 (Ludwig 2001), by J. Wooden at the SUMAC, using the methods of Williams (1997) and Ireland and Williams (2003). Common lead corrections were achieved by model age curve fitting of the uncorrected analytical data to Stacey and Kramers's (1975) lead evolution model. Results were calibrated relative to the zircon standard R33, a 419-Ma quartz diorite of the Braintree complex (Black et al. 2004). Initial calibration of the instrument was performed by analyzing four or five R33 grains at the beginning of the analytical run for each new grain mount, with calibration checks performed throughout the session by analysis of an R33 grain after every four or five unknowns. Zircons from six phonolite samples were analyzed during analytical sessions in 2004–2006. Relative to the accepted value of 419 Ma, 18 analyses of R33 produced an average of 418.9 ± 2.1 Ma during 2004, 15 analyses produced an average of 419.0 ± 2.7 Ma during 2005, and 15 analyses produced an average of 418.9 ± 3.5 Ma during 2006 (tables A1, A2, available in the online edition or from the *Journal of Geology* office). Analytical spots were chosen on individual grains according to zircon morphology, the surface texture as revealed in the reflected light images, and the zo-

Table 1. U-Pb SHRIMP-RG Results from Zircon Grains Recovered from Balcones Igneous Province Samples

Sample, grain and spot no.	Comm. ^{206}Pb (%)	U (ppm)	Th (ppm)	$^{232}Th/^{238}U$	^{204}Pb-corrected $^{206}Pb/^{238}U$ age (1σ; Ma)	^{207}Pb-corrected $^{206}Pb/^{238}U$ age (1σ; Ma)	^{208}Pb-corrected $^{206}Pb/^{238}U$ age (1σ; Ma)	^{204}Pb-corrected $^{207}Pb/^{206}Pb$ age (1σ; Ma)	^{204}Pb-corrected $^{208}Pb/^{232}Th$ age (1σ; Ma)	Total $^{238}U/^{206}Pb$ (% error)	Total $^{207}Pb/^{206}Pb$ (% error)	^{204}Pb-corrected $^{238}U/^{206}Pb$ (% error)	^{204}Pb-corrected $^{207}Pb/^{206}Pb$ (% error)	^{204}Pb-corrected $^{207}Pb/^{235}U$ (% error)	^{204}Pb-corrected $^{206}Pb/^{238}U$ (% error)	^{204}Pb-corrected Error correlation coefficient	Concordia age (Ma)
G-UV01:																	
1.1	.45	48	18	.39	681.5 (8.9)	684.2 (8.3)	685.3 (8.6)	558 (192)	614 (74)	8.89 (1.2)	.07 (2.3)	8.97 (1.4)	.0588 (8.8)	.90 (8.9)	.1115 (1.4)	.154	681.1 ± 8.9
G-UV03:																	
1.1	1.35	1088	2245	2.13	77.3 (.8)	76.9 (.8)	76.6 (1.3)	234 (126)	79 (1)	82.17 (1.0)	.06 (1.8)	82.95 (1.0)	.0508 (5.5)	.08 (5.6)	.0121 (1.0)	.184	77.2 ± 1.6
2.1	.10	289	284	1.02	77.9 (1.2)	77.1 (1.1)	76.6 (1.3)	450 (208)	85 (4)	83.01 (1.4)	.05 (3.6)	82.22 (1.5)	.0559 (9.4)	.09 (9.5)	.0122 (1.5)	.158	77.9 ± 2.3
3.1	.00	1762	2945	1.73	77.0 (.7)	77.0 (.7)	76.6 (1.0)	85 (34)	78 (1)	83.25 (.9)	.05 (1.5)	83.24 (.9)	.0477 (1.4)	.08 (1.7)	.0120 (.9)	.524	77.0 ± 1.4
4.1	.18	1298	1705	1.36	77.9 (.7)	77.9 (.7)	77.7 (1.0)	70 (55)	79 (1)	82.09 (.9)	.05 (1.7)	82.26 (.9)	.0474 (2.3)	.08 (2.5)	.0122 (.9)	.377	77.9 ± 1.5
5.1	.14	4468	7615	1.76	80.5 (.7)	80.4 (.7)	80.7 (.9)	137 (21)	80 (1)	79.61 (.8)	.05 (.9)	79.61 (.8)	.0488 (.9)	.08 (1.2)	.0126 (.8)	.676	Hi U
6.1	.49	544	98	.19	75.9 (.8)	75.8 (.8)	75.9 (.9)	128 (100)	78 (6)	84.10 (1.1)	.05 (2.4)	84.40 (1.1)	.0486 (4.3)	.08 (4.4)	.0118 (1.1)	.255	75.9 ± 1.7
7.1	.29	154	142	.96	78.6 (1.3)	78.0 (1.3)	76.9 (1.6)	387 (153)	89 (4)	81.96 (1.7)	.05 (4.7)	81.49 (1.7)	.0544 (6.8)	.09 (7.0)	.0123 (1.7)	.246	78.6 ± 2.7
8.1	.12	175	271	1.60	77.9 (1.2)	77.7 (1.3)	77.6 (1.8)	182 (102)	79 (2)	82.35 (1.6)	.05 (4.5)	82.22 (1.6)	.0497 (4.4)	.08 (4.7)	.0122 (1.6)	.346	77.9 ± 2.5
9.1	.15	399	351	.91	76.8 (1.0)	77.0 (1.0)	76.7 (1.2)	−34 (116)	77 (2)	83.09 (1.3)	.05 (2.9)	83.43 (1.3)	.0454 (4.8)	.08 (5.0)	.0120 (1.3)	.264	76.8 ± 2.0
10.1	.39	483	420	.90	75.7 (.8)	75.4 (.9)	74.8 (1.0)	241 (74)	82 (2)	84.71 (1.1)	.05 (3.2)	84.67 (1.1)	.0510 (3.2)	.08 (3.4)	.0118 (1.1)	.331	75.7 ± 23
11.1	−.08	2453	3886	1.64	79.8 (.7)	79.9 (.7)	79.5 (1.0)	19 (33)	81 (1)	80.27 (.9)	.05 (1.3)	80.33 (.9)	.0464 (1.4)	.08 (1.7)	.0124 (.9)	.563	Hi U
12.1	.38	365	536	1.52	77.4 (.9)	77.4 (.9)	76.7 (1.3)	63 (118)	80 (2)	82.44 (1.2)	.05 (2.9)	82.79 (1.2)	.0473 (4.9)	.08 (5.1)	.0121 (1.2)	.243	77.4 ± 1.9
G−UV05:																	
1.1	.45	293	672	2.37	76.7 (1.1)	77.8 (1.0)	77.3 (1.9)	−618 (361)	76 (2)	81.97 (1.3)	.05 (3.3)	83.52 (1.4)	.0362 (13.2)	.06 (13.3)	.0120 (1.4)	.107	76.6 ± 33
2.1	.28	731	381	.54	77.0 (.9)	76.8 (.9)	77.5 (1.0)	144 (82)	71 (2)	83.15 (1.2)	.05 (3.1)	83.24 (1.2)	.0489 (3.5)	.08 (3.7)	.0120 (1.2)	.322	77.0 ± 1.8
3.1	.15	1257	1362	1.12	77.6 (.7)	77.6 (.7)	77.5 (.9)	50 (59)	78 (1)	82.41 (.9)	.05 (1.6)	82.59 (.9)	.0470 (2.5)	.08 (2.6)	.0121 (.9)	.351	77 ± 1.4
4.1	.25	614	570	.96	79.3 (.8)	79.3 (.9)	79.6 (1.0)	73 (72)	77 (2)	80.58 (1.1)	.05 (2.3)	80.79 (1.1)	.0475 (3.0)	.08 (3.2)	.0124 (1.1)	.335	79.3 ± 1.7
5.1	.21	827	1703	2.13	77.8 (.9)	78.0 (.9)	78.6 (1.6)	−22 (97)	76 (2)	82.02 (1.2)	.05 (2.0)	82.39 (1.2)	.0456 (4.0)	.08 (4.2)	.0121 (1.2)	.289	77.7 ± 1.9
6.1	.38	776	560	.75	77.3 (.8)	77.3 (.8)	77.1 (.9)	117 (75)	79 (2)	82.62 (1.0)	.05 (2.4)	82.85 (1.0)	.0484 (3.2)	.08 (3.3)	.0121 (1.0)	.303	77.3 ± 1.5
7.1	−.17	52	11	.22	781.3 (10.2)	786.7 (10.5)	785.0 (10.4)	580 (93)	665 (66)	7.72 (1.4)	.06 (2.1)	7.76 (1.4)	.0594 (4.3)	1.05 (4.5)	.1288 (1.4)	.309	778 ± 290
G-UV06:																	
1.1	.44	83	45	.56	978.7 (8.4)	978.6 (8.5)	984.0 (9.0)	982 (62)	914 (33)	6.07 (.9)	.08 (1.3)	6.10 (.9)	.0719 (3.0)	1.62 (3.2)	.1640 (.9)	.291	978.8 ± 8.4
2.1	−.05	398	186	.48	83.7 (.9)	84.5 (.7)	84.2 (.8)	−362 (368)	77 (8)	75.84 (.9)	.05 (2.7)	76.55 (1.1)	.0398 (14.2)	.07 (14.2)	.0131 (1.1)	.077	83.64 ± 16
3.1	.19	116	53	.47	1018.0 (7.3)	1013.1 (7.5)	1015.2 (7.7)	1130 (36)	1060 (26)	5.87 (.8)	.07 (1.1)	5.85 (.8)	.0773 (1.8)	1.82 (2.0)	.1711 (.8)	.393	Discordant

G-UV15:																	
1.1	−.27	856	721	.87	76.5 (.9)	76.7 (1.0)	76.4 (1.1)	−33 (70)	77 (2)	83.76 (1.2)	.05 (2.9)	83.76 (1.2)	.0454 (2.9)	.07 (3.2)	.0119 (1.2)	.393	76.5 ± 1.9
2.1	.11	2097	1915	.94	80.9 (.9)	81.0 (.9)	80.3 (1.2)	53 (51)	85 (2)	79.01 (1.2)	.05 (1.6)	79.15 (1.2)	.0471 (2.1)	.08 (2.4)	.0126 (1.2)	.476	Hi U
3.1	1.01	1336	579	.45	79.3 (1.0)	79.4 (1.0)	79.2 (1.0)	18 (132)	80 (4)	79.90 (1.2)	.06 (1.8)	80.83 (1.2)	.0464 (5.5)	.08 (5.6)	.0124 (1.2)	.219	79.3 ± 1.9
4.1	.47	129	65	.52	74.0 (1.6)	75.4 (1.4)	75.4 (1.6)	−935 (922)	58 (12)	84.57 (1.8)	.05 (6.0)	86.60 (2.2)	.0323 (31.5)	.05 (31.6)	.0115 (2.2)	.069	73.9 ± 3.2
5.1	−.54	37	5	.15	73.1 (2.2)	73.5 (2.3)	72.7 (2.3)	−157 (334)	90 (14)	87.65 (3.1)	.04 (13.4)	87.65 (3.1)	.0432 (13.4)	.07 (13.8)	.0114 (3.1)	.223	73.1 ± 4.5
6.1	1.24	32	4	.12	75.7 (3.2)	78.9 (2.6)	79.3 (2.6)	…	…	80.22 (3.2)	.06 (11.4)	84.62 (4.2)	…	…	.0118 (4.2)	…	…
7.1	−.06	26	6	.22	79.8 (2.8)	79.9 (2.9)	76.9 (3.0)	58 (341)	164 (20)	80.27 (3.5)	.05 (14.3)	80.27 (3.5)	.0472 (14.3)	.08 (14.7)	.0125 (3.5)	.237	79.8 ± 5.6
8.1	.11	754	209	.29	78.3 (1.0)	78.2 (1.0)	78.5 (1.0)	122 (73)	74 (2)	81.80 (1.3)	.05 (3.1)	81.80 (1.3)	.0485 (3.1)	.08 (3.3)	.0122 (1.3)	.384	78.3 ± 2.0
9.1	.28	767	55	.07	75.3 (1.0)	75.2 (1.0)	75.4 (1.0)	130 (73)	64 (7)	85.04 (1.3)	.05 (2.6)	85.16 (1.3)	.0486 (3.1)	.08 (3.3)	.0117 (1.3)	.382	75.3 ± 1.9
10.10	−.14	1202	1077	.93	81.8 (1.0)	82.1 (1.0)	81.9 (1.2)	−71 (70)	81 (2)	78.10 (1.2)	.05 (2.1)	78.28 (1.2)	.0447 (2.9)	.08 (3.1)	.0128 (1.2)	.391	Hi Th/U
11.10	.09	1611	598	.38	78.9 (.9)	78.7 (.9)	78.7 (1.0)	209 (61)	83 (2)	81.37 (1.2)	.05 (1.8)	81.16 (1.2)	.0503 (2.6)	.09 (2.9)	.0123 (1.2)	.413	78.9 ± 24
12.10	1.18	52	7	.13	77.0 (2.0)	76.1 (2.0)	76.7 (2.1)	486 (199)	92 (13)	83.26 (2.6)	.06 (9.0)	83.26 (2.6)	.0569 (9.0)	.09 (9.4)	.0120 (2.6)	.278	76.8 ± 4.0
13.10	1.71	54	7	.13	83.8 (3.6)	76.4 (2.1)	77.4 (2.1)	1914 (408)	390 (160)	82.40 (2.6)	.06 (9.3)	76.47 (4.4)	.1172 (22.8)	.21 (23.2)	.0131 (4.4)	.189	82.7 ± 120
14.10	.15	1115	934	.87	75.9 (.9)	75.8 (.9)	75.9 (1.1)	97 (73)	76 (1)	84.38 (1.2)	.05 (2.9)	84.46 (1.2)	.0479 (3.1)	.08 (3.3)	.0118 (1.2)	.370	75.9 ± 1.9
15.10	.18	786	205	.27	78.9 (1.0)	78.9 (1.0)	79.2 (1.0)	79 (71)	73 (3)	81.01 (1.3)	.05 (2.5)	81.15 (1.3)	.0476 (3.0)	.08 (3.2)	.0123 (1.3)	.390	78.9 ± 2.0
16.10	.03	1691	1919	1.17	81.0 (1.0)	80.9 (1.0)	80.6 (1.2)	95 (41)	83 (1)	79.12 (1.2)	.05 (1.7)	79.12 (1.2)	.0479 (1.7)	.08 (2.1)	.0126 (1.2)	.562	Hi U
17.10	.04	95	52	.56	73.3 (1.7)	74.9 (1.6)	75.1 (1.8)		54 (10)	85.53 (2.1)	.05 (7.5)	87.48 (2.4)	.0298 (33.4)	.05 (33.5)	.0114 (2.4)	.071	73.1 ± 3.2
18.10	.10	426	117	.28	82.4 (1.2)	82.0 (1.2)	82.0 (1.2)	289 (110)	93 (6)	78.06 (1.4)	.05 (3.6)	77.70 (1.4)	.0521 (4.8)	.09 (5.0)	.0129 (1.4)	.284	Discordant
19.10	.38	88	24	.28	78.5 (1.8)	79.1 (1.7)	79.5 (1.8)	−279 (452)	56 (15)	80.67 (2.2)	.05 (7.5)	81.63 (2.3)	.0411 (17.8)	.07 (17.9)	.0122 (2.3)	.128	78.4 ± 3.6
20.10	.37	293	112	.39	78.2 (1.2)	78.2 (1.2)	78.7 (1.3)	77 (144)	71 (4)	81.60 (1.5)	.05 (4.2)	81.90 (1.5)	.0475 (6.0)	.08 (6.2)	.0122 (1.5)	.246	78.2 ± 2.4
21.10	1.14	45	12	.28	74.7 (2.1)	73.8 (2.1)	74.9 (2.2)	472 (221)	71 (8)	85.82 (2.8)	.06 (10.0)	85.82 (2.8)	.0565 (10.0)	.09 (10.4)	.0117 (2.8)	.268	74.6 ± 4.1
22.10	−.12	737	377	.53	77.6 (1.0)	77.9 (1.0)	77.7 (1.1)	−85 (102)	76 (3)	82.34 (1.3)	.05 (2.6)	82.56 (1.3)	.0445 (4.2)	.07 (4.3)	.0121 (1.3)	.294	77.26 ± 2.0
23.10	.44	396	23	.06	80.5 (1.1)	80.6 (1.1)	80.9 (1.1)	21 (153)	35 (26)	79.13 (1.4)	.05 (3.5)	79.60 (1.4)	.0464 (6.4)	.08 (6.5)	.0126 (1.4)	.218	80.5 ± 2.3
24.10	.21	1003	220	.23	77.5 (.9)	77.3 (1.0)	77.3 (1.0)	158 (52)	82 (2)	82.72 (1.2)	.05 (2.2)	82.72 (1.2)	.0492 (2.2)	.08 (2.5)	.0121 (1.2)	.483	77.5 ± 1.9
G-UV16:																	
1.1	.31	479	317	.68	81.2 (1.1)	81.5 (1.1)	81.2 (1.3)	−56 (169)	81 (3)	78.39 (1.4)	.05 (4.0)	78.89 (1.4)	.0450 (6.9)	.08 (7.1)	.0127 (1.4)	.196	81.2 ± 2.2
2.1	.09	812	316	.40	76.2 (1.0)	76.3 (1.0)	76.0 (1.0)	46 (80)	80 (3)	83.93 (1.3)	.05 (2.5)	84.07 (1.3)	.0469 (3.3)	.08 (3.6)	.0119 (1.3)	.355	76.2 ± 1.9
3.1	.38	924	1264	1.41	94.1 (1.3)	94.6 (1.3)	94.1 (1.7)	−165 (208)	94 (3)	67.37 (1.3)	.05 (3.0)	68.04 (1.4)	.0430 (8.3)	.09 (8.5)	.0147 (1.4)	.163	94.0 ± 2.6
G-UV26:																	
1.1	1.32	37	29	.81	1607.2 (26.0)	1588.3 (28.3)	1610.7 (29.1)	1791 (32)	1574 (39)	3.53 (1.8)	.11 (1.8)	3.53 (1.8)	.1095 (1.8)	4.28 (2.5)	.2831 (1.8)	.720	Discordant
2.1	−.20	135	60	.46	787.2 (10.1)	790.8 (10.4)	787.4 (10.8)	657 (56)	784 (23)	7.68 (1.4)	.06 (1.7)	7.70 (1.4)	.0615 (2.6)	1.10 (2.9)	.1299 (1.4)	.463	782 ± 300
3.1	.20	108	51	.49	783.1 (10.4)	783.2 (10.7)	783.8 (11.2)	779 (64)	774 (27)	7.73 (1.4)	.07 (1.9)	7.74 (1.4)	.0652 (3.0)	1.16 (3.3)	.1292 (1.4)	.423	783 ± 21

Table 2. $^{40}Ar/^{39}Ar$ Results from Amphibole, Phlogopite, and Nepheline-K-Feldspar Mineral Separates from Balcones Igneous Province Samples, with Applicable Notes

Sample	Lithology	Mineral	Run no.	mg	wt% K	t_{int} (Ma)	t_p (Ma)	^{39}Ar released (%)	t_{ic} (Ma)	MSWD
G-UV03	Phonotephrite	Amphibole	71C47	6.73	.2	77.8	77.4 ± 1.2	67	79.8 ± 1.7	26
G-UV05	Phonolite	Amphibole	72B21	9.5	.9	76.9	76.2 ± .6	82	76.0 ± .5	5
G-UV10	Phonolite	Amphibole	77A2	1.41	1.1	77.9	78.0 ± 1.3	96	77.3 ± .8	1
G-UV10	Phonolite	Amphibole	77A2				77.6 ± .7	66		
G-UV16	Phonolite	Amphibole	77A3	5.89	.96	78.6	78.4 ± .8	97	77.8 ± .7	2
G-UV16	Phonolite	Amphibole	77A3				78.1 ± .4	60		
G-410	Phonolite	Amphibole	72B17	4.36	1.2	71.6	76.3 ± .4	49	76.4 ± .7	5
G-UV26	Phonolite	Amphibole	77A5	5.78	1.1	77.9	77.2 ± .6	97	76.9 ± .6	2
G-UV26	Phonolite	Amphibole	77A5				77.0 ± .3	71		
G-UV30	Olivine nephelinite	Biotite	77A6	3.88	5	83.4	83.5 ± .5	75	83.9 ± .5	2
G-UV33	Nepheline basanite	Biotite	77A7	5.3	5.5	83.1	83.5 ± .5	86	83.6 ± .6	2
G-UV34	Nepheline basanite	Biotite	77A8	.37	5.5	81.5	81.5 ± 1.6	85	81.3 ± 2.8	2
G-UV03	Phonotephrite	Nepheline-K-feldspar concentrate	71C48	5.13	4.3	73.1	74.4 ± .4	56	74.0 ± .8	60
G-UV03	Phonotephrite	Nepheline-K-feldspar concentrate	71C49	10.4	3.9	73.0	74.8 ± .4	55	73.5 ± 1.1	204

Note. t_{int} = integrated (or total-gas) age; derived from the summation of all fractions of the incremental-heating analysis. t_p = plateau age; derived from the incremental-heating age spectrum. All quoted age uncertainties are at the 2σ level. t_{ic} = isotope-correlation age; derived from the $^{36}Ar/^{40}Ar$ versus $^{39}Ar/^{40}Ar$ regression. The reliability of the listed age must be evaluated the MSWD, amounts of Ar, number of gas fractions used, and general age spectrum results. These regressions are included to augment and illustrate the general release pattern but generally do not provide more reliable ages than the age spectra.

nation of each zircon as revealed in CL images (fig. 3). Spots were chosen to avoid cracks and especially dark (high-uranium) or bright (low-uranium) zones within each grain. Analytical results for U-Pb analyses of zircons for the BIP samples are summarized in table 1.

The $^{40}Ar/^{39}Ar$ measurements were performed in the Radiogenic Isotopes Laboratory at Ohio State University. The general procedures have been described previously (see Foland et al. 1993 and references therein), except for the use of a new noble-gas mass analysis system. Sized aliquots of phlogopite and amphibole separates were irradiated under a high neutron flux for about 25 h in the McMaster Nuclear Reactor at McMaster University in Hamilton, Ontario. The aliquots were subsequently heated incrementally to successively higher temperatures, using a custom-built, resistance-heating, high-vacuum, and low-blank furnace. Step-heating was continuous, with ramp times from one temperature to another of about 1 min and with dwell times of about 30 min at each temperature. These incremental-heating fractions, typically about 20–25 steps, were analyzed by static-gas mass analysis with a MAP 215-50 mass spectrometer.

Corrections for interfering reactions producing Ar from K, Ca, and Cl were made using factors determined from interference monitors that were irradiated along with the mineral aliquots. The age monitor used was an intralaboratory muscovite standard (PM-1) that has a $^{40}Ar/^{39}Ar$ age of 165.3 Ma; an uncertainty of ±1% is assigned to this age in order to allow for uncertainties in the standards against which PM-1 was calibrated. The age for this monitor was determined by simultaneous cross-calibration with several monitors, including the Fish Canyon Tuff biotite standard (FCT-3), with an age of 27.84 Ma. All factors and constants are provided in table A3, available in the online edition or from the *Journal of Geology* office.

Three kinds of $^{40}Ar/^{39}Ar$ ages are reported in table 2. The total gas age (t_{int}) represents an integrated age derived by summing all gas fractions. Total plateau age (t_p) is determined by heating the sample to a given temperature and deriving an apparent age from the gas fraction released. A series of heating steps at increasing temperature produces a series of gas release increments through which isochrons are drawn. Meaningful plateau ages must have the following characteristics: (1) plateau gas ages must be well-defined plateaus by contiguous release of >50% of total ^{39}Ar, (2) plateau gas fractions must form well-defined isochrons, (3) isochron ages and plateaus must be concordant, and (4) $^{40}Ar/^{36}Ar$ must not differ significantly from the atmospheric value of 295.5 ± 0.5 (Lanphere 1999). Isotope correlation, or reverse isochron, age (t_{ic}) is derived by plotting $^{36}Ar/^{40}Ar$ versus $^{39}Ar/^{40}Ar$. With the ordinate intercept representing the inverse of the atmospheric Ar ratio and the abscissa intercept representing the $^{39}Ar/^{40}Ar$ released during the heat-

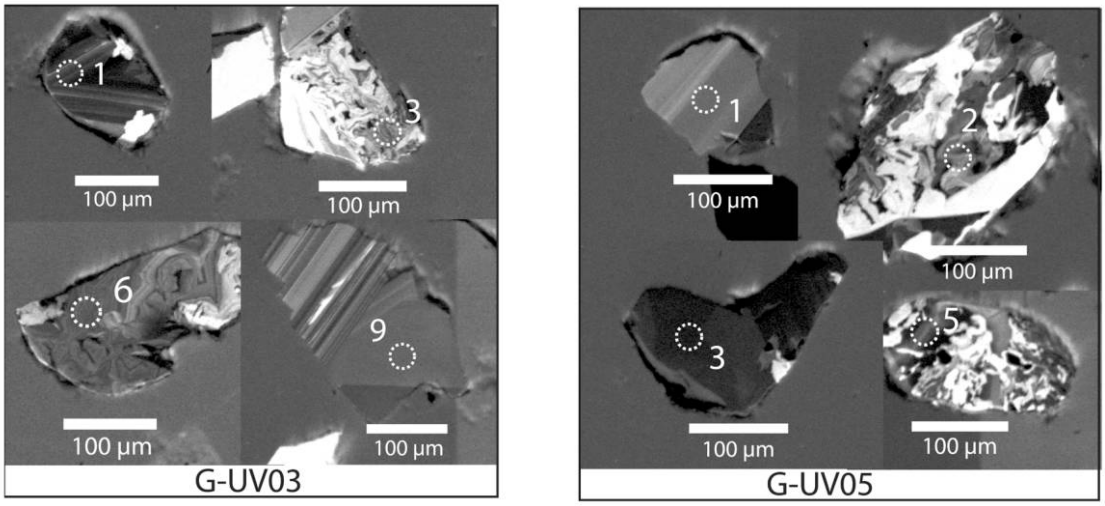

Figure 3. Cathode luminescence images of typical zircon grains from Balcones igneous province samples. Dashed circles represent the ion ablation spots from which ages were derived. Zircon grains exhibited normal compositional banding (G-UV03 grains 1, 9; GUV05 grains 1, 3), as well as complex compositional banding, although both types produced concordant ages.

ing steps, ages are derived from the slope of the isochron. The t_p ages provide the most meaningful results because they must adhere to the previously defined criteria and are derived from a pooled age of multiple step-heating increments. Gas fractions released at the highest- and lowest-temperature steps tend to produce higher uncertainties than the intermediate heating steps and can be eliminated from the plateau age calculation (e.g., Lanphere 1999). The t_{ic} ages are not as precise as the t_p ages because they are related to how well the isochrons fit the data. The t_{int} ages are the least preferred because they are derived from the summation of all gas release fractions and do not exclude the highest- and lowest-temperature heating steps that typically contain the greatest uncertainty.

Results

$^{40}Ar/^{39}Ar$ Geochronology. Amphiboles were separated from five phonolite and one phonotephrite sample, phlogopites were separated from one olivine nephelinite and two nepheline basanites, and a nepheline+K-feldspar concentrate was separated from a phonotephrite. Sample locations are given in table 3 and figure 2. Detailed results for the 11 analyses are listed in table A3 and shown in figure 4. Results are summarized in tables 2 and 3. Results for the 11 analyses are that all samples yielded initial $^{40}Ar/^{36}Ar$, close to atmospheric (298 ± 5, 310 ± 9, 300 ± 3, 298 ± 6, 300 ± 7, 299 + 11, 289 ± 6, 271 ± 18, 295 ± 40, 296 ± 6, and 282 ± 7). Analyses of the phonolite amphiboles produced t_{int} ages ranging from 71.6 to 77.9 Ma and an age of 77.8 Ma from the phonotephrite (fig. 4; table 2); errors are not calculated for t_{int} ages. The t_p ages ranged from 76.2 ± 0.6 to 78.4 ± 0.8 Ma (2σ) for the phonolite amphiboles, and the age was 77.4 ± 1.2 Ma (2σ) for the phonotephrite amphiboles. Plateaus range in width (total ^{39}Ar release) from a low of 49% (phonolite sample G-410; all other phonolites >60%) to 97% in amphibole from the felsic rocks. The t_{ic} ages range from 76.4 ± 0.7 (MSWD = 5) to 77.8 ± 0.7 (MSWD = 2) for the phonolites, and the age was 79.8 ± 1.7 (MSWD = 26) for the phonotephrite (fig. 4; table 2).

Phlogopite separated from two nepheline basanites produced t_{int} ages of 81.5 (initial $^{40}Ar/^{36}Ar$ = 300 ± 7) and 83.1 Ma (initial $^{40}Ar/^{36}Ar$ = 299 ± 11), t_p ages of 81.5 ± 1.6 and 83.5 ± 0.5 Ma (2σ; these plateau ages consist of 75%–86% total ^{39}Ar release), and t_{ic} ages of 81.3 ± 2.8 (MSWD = 2) and 83.6 ± 0.6 (MSWD = 2) Ma. Phlogopite separated from the olivine nephelinite produced a t_{int} age of 83.4 Ma (initial $^{40}Ar/^{36}Ar$ = 298 ± 6), a t_p age of 83.5 ± 0.5 Ma (2σ), and a t_{ic} age of 83.9 ± 0.5 Ma (MSWD = 2; fig. 4; table 2).

Nepheline separates were prepared for dating; however, the presence of K-feldspar in the more evolved phonolites made the separation difficult, owing to the common physical characteristics (sim-

Table 3. Detail of All Geochronology Results from the Balcones Igneous Province

Sample	Lithology	Fig. 2 location	$^{40}Ar/^{39}Ar$ mineral (Ma)	$^{40}Ar/^{39}Ar$ concentrate (Ma)	$^{40}K/^{40}Ar$ whole rock (Ma)	U-Pb (Ma)
G-UV01	Olivine nephelinite	1				Xenocryst
G-UV03	Phonotephrite	3	77.4 ± 1.2 amphibole	74.4 ± .4		77.26 ± .61 WMA
G-UV03	Phonotephrite	3		74.8 ± .4		
G-UV05	Phonolite	5	76.2 ± .6 amphibole			77.78 ± .74 WMA
G-UV06	Olivine nephelinite	6				Single-grain 83.64 ± 16, plus one xenocryst, one discordant
G-UV10	Phonolite	7	78.0 ± 1.3 amphibole			
G-UV10	Phonolite	7	77.6 ± .7 amphibole			
G-UV15	Phonolite	12				77.32 ± .99 WMA
G-UV16	Phonolite	13	78.4 ± .8 amphibole			76.2 ± 1.9, 81.2 ± 2.2, 94.0 ± 2.6
G-UV16	Phonolite	13	78.1 ± .4 amphibole			No coherent age group
G-410	Phonolite	49	76.3 ± .4 amphibole			
G-UV26	Phonolite	23	77.2 ± .6 amphibole			Xenocryst
G-UV26	Phonolite	23	77.0 ± .3 amphibole			
G-UV30	Olivine nephelinite	27	83.5 ± .5 phlogopite			
G-UV33	Nepheline basanite	30	83.5 ± .5 phlogopite			
G-UV34	Nepheline basanite	31	81.5 ± 1.6 phlogopite			
M-01-CB-002	Melilite olivine basanite	36		80.9 ± .6		
M-01-CB-002	Melilite olivine basanite	36		80.48 ± .29		
M-01-CB-005	Phonolite	5	72.41 ± .15 K-feldspar			

M-01-CB-005	Phonolite	5	72.60 ± .26 K-feldspar		
M-01-CB-006	Phonotephrite	3	73.39 ± .13 K-feldspar		
M-01-CB-007	Olivine nephelinite	~9		79.2 ± .6 (max)	
M-01-CB-008	Alkali basalt	~61	80.92 ± .16 plagioclase	82.79 ± .13 (min)	
M-01-CB-009	Olivine nephelinite	~28		78.9 ± 1.4	
M-01-CB-0010	Not reported	64		78.52 ± .12	
BA-KCO-2	Nepheline basanite	31			75 ± 3
BA-KCO-3	Nepheline basanite	33			82 ± 4
BA-KCO-4	Olivine nephelinite	…			88 ± 5
BA-KCO-5	Olivine nephelinite	52			79 ± 5
BA-KCO-6	Alkali basalt	65			81 ± 5
BA-KCO-6	Alkali basalt	65			80 ± 3
BA-KCO-7	Olivine nephelinite	28			75 ± 3
BA-KCO-11	Phonotephrite	3			65 ± 2
BA-KCO-12	Melilite olivine basanite	2			84 ± 4
BA-KCO-13	Phonolite	5			65 ± 2
BA-KCO-14	Nepheline basanite	25			79 ± 3
BA-KCO-15	Melilite olivine basanite	36			76 ± 3
BA-KCO-15	Melilite olivine basanite	36			77 ± 3
BA-KCO-16	Olivine nephelinite	9			84 ± 4
BA-KCO-17	Olivine nephelinite	18			78 ± 3
BA-KCO-18	Olivine nephelinite	1			86 ± 4
BA-TCO-21	Olivine nephelinite	43			80 ± 3
BD-443	Melilite olivine nephelinite	20	74.5 ± 1.5 nepheline		72.8 ± 1.5
BD-443	Melilite olivine nephelinite	20	74.9 ± 1.5 nepheline		69.7 ± 1.5
BD-443	Melilite olivine nephelinite	20	69.7 ± 5 pyroxene		
BD-443	Melilite olivine nephelinite	20	72.0 ± 5 pyroxene		
BD-562	"Limburgite"	43			69.1 ± 1.5
BD-562	"Limburgite"	43			69.3 ± 1.5

Note. Individual studies are indicated by the sample number as follows: G = this study; M = Miggins et al. (2004); BA = Baldwin and Adams (1971); and BD = Burke et al. (1969). Map locations for figure 2 are detailed, as well as the method used to derive the ages. All ages published before 1976 have been converted for new decay and abundance constants ($^{40}K/K = 1.167 \times 10^{-4}$ mol/mol; $\lambda_\beta = 4.962 \times 10^{-10}$ yr^{-1}; $\lambda_\epsilon + \lambda'_\epsilon = 0.581 \times 10^{-10}$ yr^{-1}), as suggested by the International Union of Geological Sciences Subcommission on Geochronology. An ellipsis indicates insufficient description.

ilar magnetic susceptibility, specific gravity, and color of crushed grains) of both nepheline and K-feldspar. No nepheline separates could be purified sufficiently to provide a viable target for phonolite dating. The results of five analytical runs produced t_{int} ages (errors are not calculated) of 69.6, 63.6, 48.1, and 45.9 Ma (not shown). The t_p and t_{ic} ages were not calculated because all were clearly too young, as indicated by the fact that coexisting amphibole t_{int} separate ages of >76 Ma were obtained for some of these samples. The results of one nepheline-K-feldspar concentrate produced for phonotephrite sample G-UV03 yielded results that were only slightly younger than those for amphibole separates from the same sample (t_p amphibole age of 76.2 ± 0.6 Ma vs. t_p ages of 74.4 ± 0.4 and 74.8 ± 0.4 Ma [2σ] for the nepheline-K-feldspar concentrates), as compared with the more evolved phonolite samples discussed above (fig. 4; table 2).

Comparisons of plateau widths and ages for phlogopite, amphibole, and nepheline-K-feldspar indicate that reliable ages were obtained for all samples, on the basis of gas fraction plateau widths 60%–97%, with the exception of amphibole from phonolite G-410, with a 49% plateau width. Younger ages and more complex spectra (especially at the lowest- or highest-temperature steps) were obtained for amphibole and nepheline+K-feldspar. Overall results from the nepheline+K-feldspar dating experiment, coupled with the observation that these phases contain a very high proportion of the potassium in BIP samples (whole rock: 0.04–1.65 wt% K_2O mafic and 3.05–5.34 wt% K_2O felsic; nepheline: 2.44–12.53 wt% K_2O; K-feldspar: 2.54–11.71 wt% K_2O), indicate that whole-rock $^{40}Ar/^{39}Ar$ and $^{40}Ar/^{40}K$ dating of BIP samples is likely to yield ages that are significantly younger than the true eruption/intrusion/cooling age, explaining the younger ages of Burke et al. (1969), Baldwin and Adams (1971), and Miggins et al. (2004). The felsic samples are especially prone to age underestimation using whole-rock, groundmass, and nepheline-K-feldspar concentrates because nepheline and K-feldspar comprise significant proportions of those rocks; the mafic rocks are somewhat less susceptible to these problems because nepheline makes up a much smaller proportion of the rocks and K-feldspar is not present.

U-Pb Geochronology. Zircons were separated from five phonolites and two nephelinites. Sample locations are given in table 3 and figure 2. Detailed results for all 11 analyses are listed in table 1, and $^{207}Pb/^{235}U$ versus $^{206}Pb/^{238}U$ concordia plots are shown in figure 5 for the three samples with well-constrained weighted mean ages (WMAs). All results are summarized in table 3. CL images for two samples (fig. 3) show typical zircons used for analysis; the dashed circles (20–40 μm) closely approximate the location where the ion beam sputtered a 1–2-μm-deep pit. Numbers on each grain correspond to the grain number for each sample in table 1. Dark zones within the zircons represent areas of higher U concentration relative to lighter zones. Analytical spots were chosen to avoid obvious cracks and zones of high or low U concentration. Some zircons exhibit complex internal zonation patterns; however, those grains produced ages indistinguishable from those of the regular zoned grains (table 1). Individual zircon grains exhibiting ^{204}Pb-corrected $^{207}Pb/^{235}U$ errors >10% or high U concentrations were excluded from age calculations. Analyses of 14 zircons from G-UV03 produced a 12-grain ^{204}Pb-corrected $^{206}Pb/^{238}U$ versus $^{207}Pb/^{235}U$ concordia WMA of 77.09 ± 0.57 Ma (2σ), with an MSWD of 2.0 (grains 5.1 and 11.1 were excluded because of high U concentrations); however, an 11-grain WMA age of 77.26 ± 0.61 Ma (2σ), with an MSWD of 0.63, results from exclusion of grain 10.1, which has a concordant age but a larger error of 75.7 ± 23.0 Ma (2σ), with an MSWD of 4.5 (fig. 5; table 1). Analyses of seven zircons from sample G-UV05 produced a six-grain ^{204}Pb-corrected $^{206}Pb/^{238}U$ versus $^{207}Pb/^{235}U$ concordia WMA age of 77.66 ± 0.70 Ma (2σ; MSWD of 0.22; grain 7.1 was excluded because of a clearly xenocrystic concordia age of 778 ± 290 Ma); however, a five-grain WMA age of 77.78 ± 0.74 Ma (2σ), with an MSWD of 0.021, results from the exclusion of grain 1.1, which

Figure 4. $^{40}Ar/^{39}Ar$ plateau age spectra and reverse isochron plots for Balcones igneous province samples. Three following ages are given: total plateau (t_p), total gas (t_{int}), and reverse isochron (t_{ic}). The t_p ages are preferred because they must meet preexisting criteria to provide geologically meaningful results. The t_{int} ages do not allow for exclusion of complex heating steps. The t_{ic} ages are related to the degree of fit for the isochron. The arrows on the isochron plots refer to the initial ratio of $^{40}Ar/^{36}Ar$. Filled triangles are used in determining reverse isochron ages; open triangles have been excluded from the age determination. (Figure begins on p. 13 and continues on p. 14.)

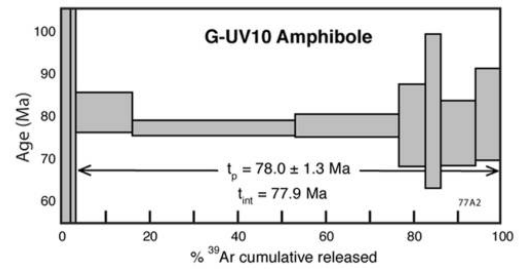
G-UV10 Amphibole
Age (Ma)
t_p = 78.0 ± 1.3 Ma
t_{int} = 77.9 Ma
77A2
% ^{39}Ar cumulative released

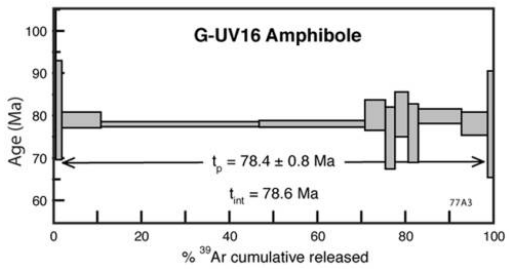
G-UV16 Amphibole
Age (Ma)
t_p = 78.4 ± 0.8 Ma
t_{int} = 78.6 Ma
77A3
% ^{39}Ar cumulative released

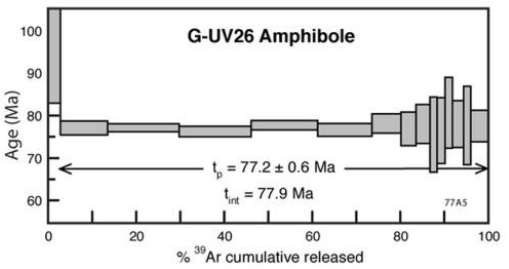
G-UV26 Amphibole
Age (Ma)
t_p = 77.2 ± 0.6 Ma
t_{int} = 77.9 Ma
77A5
% ^{39}Ar cumulative released

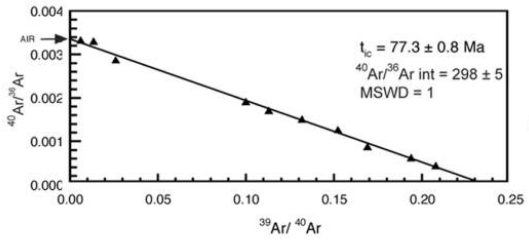
AIR
t_{ic} = 77.3 ± 0.8 Ma
^{40}Ar/^{36}Ar int = 298 ± 5
MSWD = 1
^{40}Ar/^{36}Ar
^{39}Ar/ ^{40}Ar

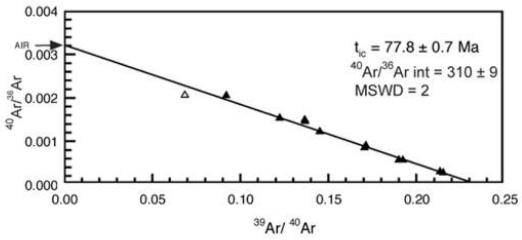
AIR
t_{ic} = 77.8 ± 0.7 Ma
^{40}Ar/^{36}Ar int = 310 ± 9
MSWD = 2
^{40}Ar/^{36}Ar
^{39}Ar/ ^{40}Ar

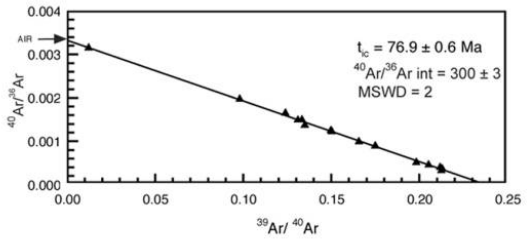
AIR
t_{ic} = 76.9 ± 0.6 Ma
^{40}Ar/^{36}Ar int = 300 ± 3
MSWD = 2
^{40}Ar/^{36}Ar
^{39}Ar/ ^{40}Ar

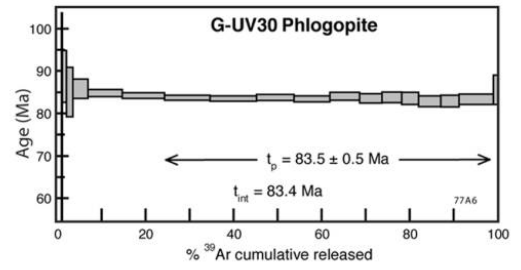
G-UV30 Phlogopite
Age (Ma)
t_p = 83.5 ± 0.5 Ma
t_{int} = 83.4 Ma
77A6
% ^{39}Ar cumulative released

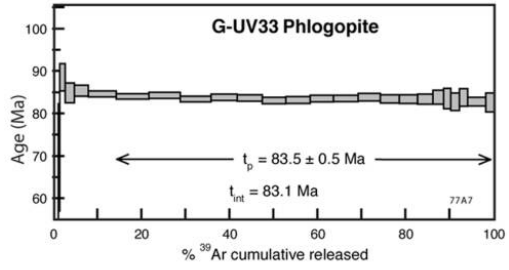
G-UV33 Phlogopite
Age (Ma)
t_p = 83.5 ± 0.5 Ma
t_{int} = 83.1 Ma
77A7
% ^{39}Ar cumulative released

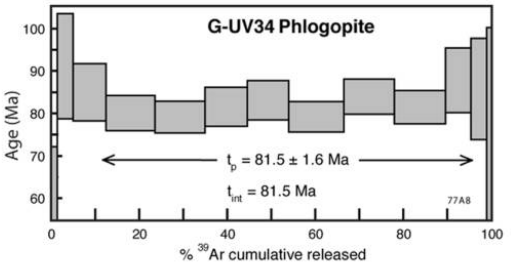
G-UV34 Phlogopite
Age (Ma)
t_p = 81.5 ± 1.6 Ma
t_{int} = 81.5 Ma
77A8
% ^{39}Ar cumulative released

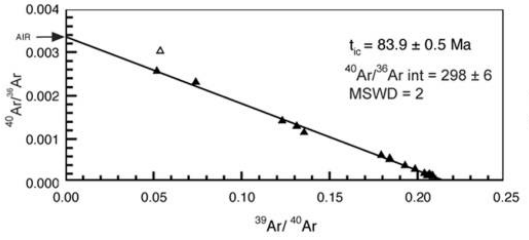
AIR
t_{ic} = 83.9 ± 0.5 Ma
^{40}Ar/^{36}Ar int = 298 ± 6
MSWD = 2
^{40}Ar/^{36}Ar
^{39}Ar/ ^{40}Ar

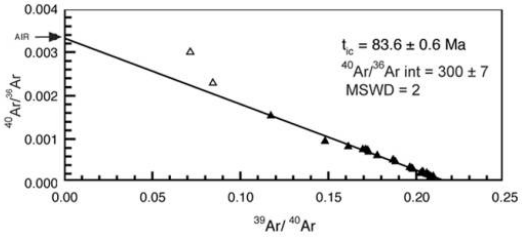
AIR
t_{ic} = 83.6 ± 0.6 Ma
^{40}Ar/^{36}Ar int = 300 ± 7
MSWD = 2
^{40}Ar/^{36}Ar
^{39}Ar/ ^{40}Ar

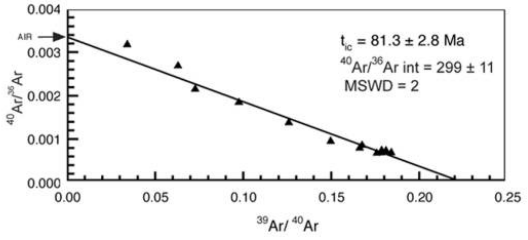
AIR
t_{ic} = 81.3 ± 2.8 Ma
^{40}Ar/^{36}Ar int = 299 ± 11
MSWD = 2
^{40}Ar/^{36}Ar
^{39}Ar/ ^{40}Ar

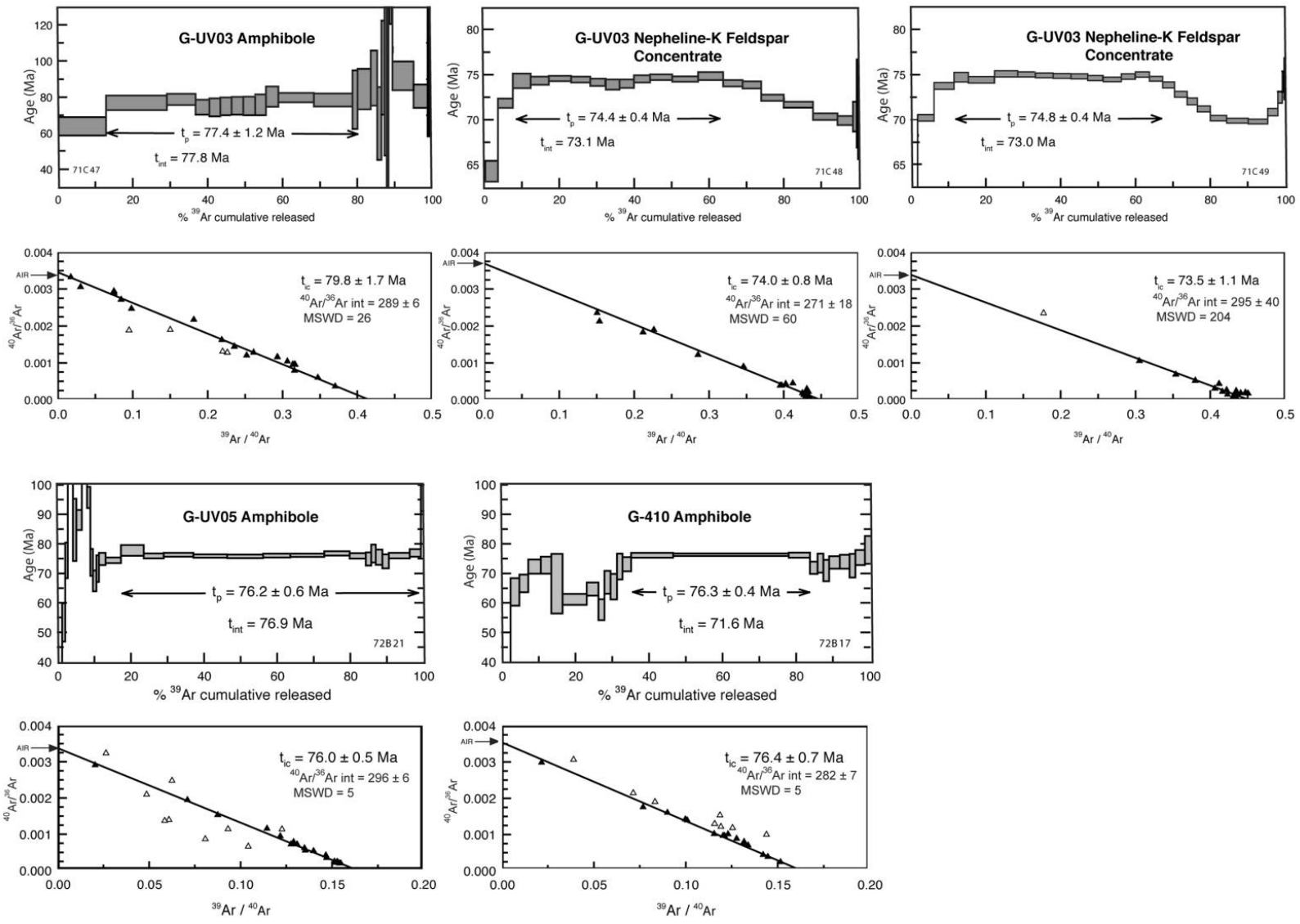
G-UV03 Amphibole
Age (Ma)
t_p = 77.4 ± 1.2 Ma
t_{int} = 77.8 Ma
71C47
% ^{39}Ar cumulative released
G-UV03 Nepheline-K Feldspar Concentrate
t_p = 74.4 ± 0.4 Ma
t_{int} = 73.1 Ma
71C48
G-UV03 Nepheline-K Feldspar Concentrate
t_p = 74.8 ± 0.4 Ma
t_{int} = 73.0 Ma
71C49
t_{ic} = 79.8 ± 1.7 Ma
^{40}Ar/^{36}Ar int = 289 ± 6
MSWD = 26
AIR
^{40}Ar/^{36}Ar
^{39}Ar / ^{40}Ar
t_{ic} = 74.0 ± 0.8 Ma
^{40}Ar/^{36}Ar int = 271 ± 18
MSWD = 60
t_{ic} = 73.5 ± 1.1 Ma
^{40}Ar/^{36}Ar int = 295 ± 40
MSWD = 204
G-UV05 Amphibole
t_p = 76.2 ± 0.6 Ma
t_{int} = 76.9 Ma
72B21
G-410 Amphibole
t_p = 76.3 ± 0.4 Ma
t_{int} = 71.6 Ma
72B17
t_{ic} = 76.0 ± 0.5 Ma
^{40}Ar/^{36}Ar int = 296 ± 6
MSWD = 5
t_{ic} = 76.4 ± 0.7 Ma
^{40}Ar/^{36}Ar int = 282 ± 7
MSWD = 5

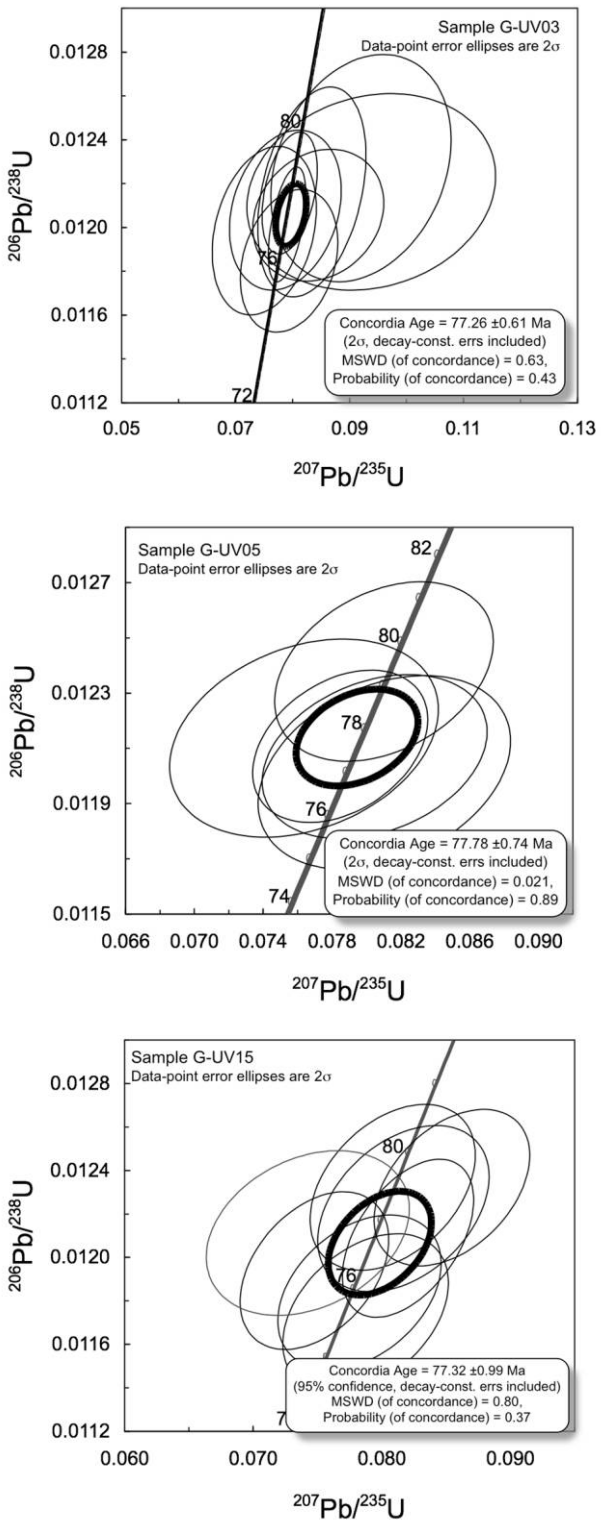

Figure 5. U-Pb weighted mean age plots for zircons from the Balcones igneous province, detailing concordia age, error, MSWD, and probability of concordance.

has a concordant age but a larger error of 76.6 ± 33.0 Ma at a 95% confidence interval, with an MSWD of 5.6 (fig. 5; table 1). Results of 12 of 24 zircons from G-UV15 (exclusion basis of grains: 2.1, 16.1: high U content; 10.2: high Th/U; 6.1, 18.1: discordant; 4.1, 5.1, 7.1, 13.1, 17.1, 19.1, 21.1: ^{204}Pb-corrected ^{207}Pb/^{235}U errors >10%) yield a ^{204}Pb-corrected ^{206}Pb/^{238}U versus ^{207}Pb/^{235}U concordia WMA age of 77.32 ± 0.99 Ma, with an MSWD of 0.80 at a 95% confidence interval (fig. 5; table 1). Analyses of two zircons from G-UV26 do not yield a coherent age group: zircon grain 1.1 is discordant, but two spots (core and rim) analyzed from the other zircon grain yield a ^{204}Pb-corrected ^{206}Pb/^{238}U versus ^{207}Pb/^{235}U concordia age of 782 ± 14 Ma (2σ), with an MSWD of 3.5 (table 1). Analyses of three zircons from G-UV16 do not yield a coherent age group; however, each individual grain is concordant, resulting in ^{204}Pb-corrected ^{206}Pb/^{238}U versus ^{207}Pb/^{235}U concordia ages of 81.2 ± 2.2, 76.2 ± 1.9, and 94.0 ± 2.6 Ma (2σ), with MSWDs of 0.71, 0.14, and 1.8, respectively (table 1). Three zircons analyzed from G-UV06 do not yield a coherent age group; however, two grains yield ^{204}Pb-corrected ^{206}Pb/^{238}U versus ^{207}Pb/^{235}U concordia ages of 988.8 ± 8.4 (2σ) and 83.64 ± 16 Ma (95% confidence interval), and the third grain was discordant (^{207}Pb/^{206}Pb age of 1130 Ma; table 1). A single zircon from G-UV01 yields a ^{204}Pb-corrected ^{206}Pb/^{238}U versus ^{207}Pb/^{235}U concordia age of 681.1 Ma (2σ), with an MSWD of 1.8 (table 1).

Discussion

The geochronology results provide important constraints on the evolution of the BIP. This section first compares the different geochronological systems and shows which methods and dating targets yield the most geologically meaningful results. The proposed timing and duration of magmatism in the BIP are summarized next, and the significance of xenocrystic zircons is discussed. We then discuss the monogenetic nature of the BIP as compared with similar polygenetic magmatic provinces. We finish our discussion by exploring the mantle plume and hot spot trail hypothesis advocated by Cox and Van Arsdale (2002) as a potential magmatic mechanism for the BIP and the NGMMZ.

Comparison of Techniques. The timing and duration of BIP magmatism has not been isotopically well constrained, although three previous studies have been conducted (Burke et al. 1969; Baldwin and Adams 1971; Miggins et al. 2004). The previous results, along with those of this study, are summarized in table 3 and shown in figure 6. Ages published

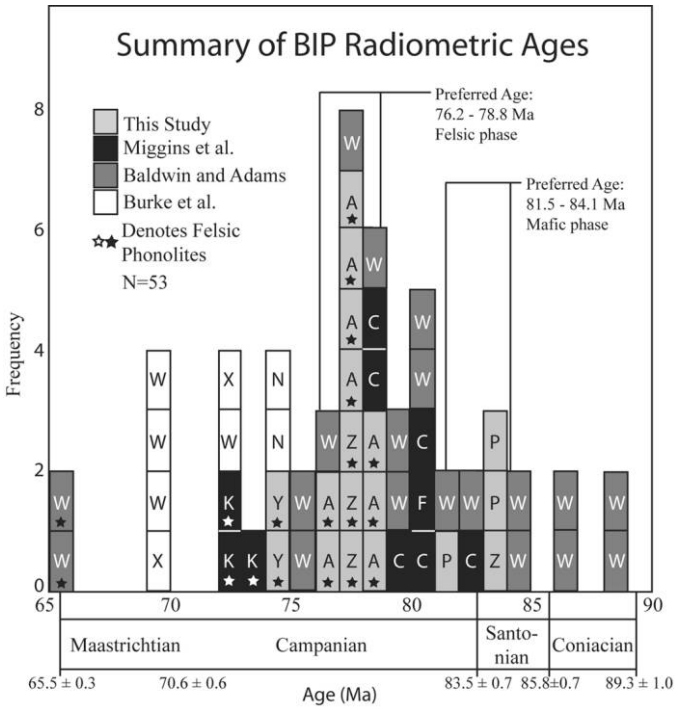

Figure 6. Histogram summarizing all isotopic ages (n = 53) calculated for samples from the Balcones igneous province, including $^{40}K/^{40}Ar$, $^{40}Ar/^{39}Ar$, and U-Pb methods. Although the histogram approximates a near-normal distribution as a whole, many of the $^{40}K/^{40}Ar$ ages are suspect.

before 1976 are converted to new decay and abundance constants ($^{40}K/K = 1.167 \times 10^{-4}$ mol/mol; $\lambda_\beta = 4.962 \times 10^{-10}$ yr^{-1}; $\lambda_\epsilon + \lambda'_\epsilon = 0.581 \times 10^{-10}$ yr^{-1}), as recommended by the International Union of Geological Sciences Subcommission on Geochronology (Dalrymple 1979).

Comparison of Different Techniques from This Study. Of the BIP samples dated using U-Pb zircon techniques, two have also been dated by $^{40}Ar/^{39}Ar$ using amphibole separates, providing a comparison between the two methods (table 3). For phonolite G-UV03, a ^{204}Pb-corrected WMA concordia age of 77.3 ± 0.6 Ma (2σ) is indistinguishable from an amphibole $^{40}Ar/^{39}Ar$ t_p age of 77.4 ± 1.2 Ma (2σ; 67% ^{39}Ar release). G-UV05 produced a ^{204}Pb-corrected WMA concordia age of 77.8 ± 0.7 Ma (2σ) and a slightly younger amphibole $^{40}Ar/^{39}Ar$ t_p age of 76.2 ± 0.6 Ma (2σ; 82% ^{39}Ar release). We conclude that, considering the results of our study, the most reliable eruption/emplacement ages are given by mineral separates using U-Pb or $^{40}Ar/^{39}Ar$ methods. The use of whole-rock or mixed concentrates (especially those containing nepheline or K-feldspar in the mix) produces ages that are too young.

Comparison of Results for Common Outcrops. Several outcrops we have dated for this study have been dated by at least one of the other previously discussed geochronologic studies. We compare the results of common outcrops to ascertain the quality of the age determinations reported for three outcrops where results from earlier studies can be compared with our results: Ange siding, Mount Inge, and Pinto Mountain.

Ange siding. The Ange siding phonolite (G-UV05; fig. 2, 5) has been isotopically dated in three different studies, using a variety of targets and techniques. Baldwin and Adams (1971) provided the first $^{40}Ar/^{40}K$ results, deriving a whole-rock apparent crystallization age of 65 ± 2 Ma; this age was long considered to represent the end of igneous activity in the BIP. Miggins et al. (2004) utilized K-feldspar mineral separates to derive $^{40}Ar/^{39}Ar$ t_p ages of 72.41 ± 0.15 and 72.60 ± 0.26 Ma on two separate analytical runs, noting that the analyses pro-

duced disturbed age spectra. We dated the Ange siding outcrop using $^{40}Ar/^{39}Ar$ amphibole and U-Pb zircon techniques. Amphibole separates yield a t_{int} age of 76.9 Ma and a t_p age of 76.2 ± 0.6 Ma (2σ; 82% ^{39}Ar release). Zircon separates yield a ^{204}Pb-corrected WMA concordia age of 77.8 ± 0.7 Ma (2σ). We regard the amphibole t_p and zircon separate ages as the most reliable indicators of the crystallization age of the rock because both ages are almost the same within error but take the 77.8 ± 0.7-Ma U-Pb age as best approximating the time of emplacement and cooling. We interpret ages reported by Baldwin and Adams (1971) to be younger than the actual crystallization date by ~16% and the Miggins et al. (2004) ages by 4%–7%.

Mount Inge. The Mount Inge (G-UV03; fig. 2, *3*) outcrop has been isotopically dated by three different studies, using a variety of targets and techniques. The outcrop is a tephriphonolite and is geochemically less evolved than the phonolites exposed elsewhere in the BIP. Baldwin and Adams (1971) provided the first whole-rock $^{40}Ar/^{40}K$ results, reporting an apparent crystallization age of 65 ± 2 Ma, consistent with their results from the Ange siding outcrop and lending credence to the idea that 65 Ma marked the end of BIP volcanism. Miggins et al. (2004) reported a $^{40}Ar/^{39}Ar$ K-feldspar t_p age of 73.39 ± 0.13 Ma. We report $^{40}Ar/^{39}Ar$ results of a nepheline-K-feldspar concentrate, an amphibole separate, and a U-Pb zircon separate. The nepheline-K-feldspar concentrate yielded t_{int} ages of 73.1 and 73.0 Ma and t_p ages of 74.4 ± 0.4 and 74.8 ± 0.2 Ma (2σ; 56% and 55% ^{39}Ar release, respectively) on two separate runs, similar to Miggins et al.'s (2004) result. Amphibole separates yielded a t_{int} age of 77.8 Ma and a t_p age of 77.4 ± 1.2 Ma (2σ; 67% ^{39}Ar release). Zircon separates produced a ^{204}Pb-corrected WMA concordia age of 77.26 ± 0.61 (2σ), indistinguishable from the amphibole age and significantly older than nepheline and K-feldspar ages that we and Miggins et al. (2004) derived. We regard the amphibole t_p and zircon separate ages as the most reliable indicators of the age of crystallization because both ages are identical, within error. Baldwin and Adams's (1971) age is therefore too young by ~17%. Miggins et al.'s (2004) t_p (K-feldspar separate) age is quite comparable to our t_p (nepheline-K-feldspar concentrate) date, differing by between 1.3% and 2.0%, a small difference for similar targets between two different laboratories. Amphibole and zircon separates from our study produced t_p ages older than those of Miggins et al. (2004) by between 4% and 6%. We interpret our t_p (nepheline-K-feldspar concentrate) age also to be too young, differing by 3%–4% relative to the amphibole and zircon separate t_p ages.

Pinto Mountain. Pinto Mountain (G-UV34; fig. 2, *31*) is an outcrop of nepheline basanite in the northwest extreme of the BIP. Pinto Mountain has been dated by two isotopic studies. Baldwin and Adams (1971) reported a whole-rock $^{40}Ar/^{40}K$ age of 75 ± 3 Ma. We determined a phlogopite separate $^{40}Ar/^{39}Ar$ t_{int} age of 81.5 Ma and a t_p age of 81.5 ± 1.6 Ma (2σ; 85% ^{39}Ar release). We regard the t_p age of 81.5 Ma as the most likely crystallization age for Pinto Mountain. Baldwin and Adams's (1971) age appears to be too young by ~8%.

Timing and Duration of Magmatism in the BIP. The foregoing discussion demonstrates that U-Pb zircon ages of phonolites and $^{40}Ar/^{39}Ar$ ages of amphibole in the phonolites and phlogopite in olivine nephelinites and basanites yield the most reliable ages for eruption and cooling of the BIP. By comparison, nepheline and K-feldspar separates, groundmass separates, and whole-rock $^{40}Ar/^{39}Ar$ ages give ages that are as much as 17% younger. Because nepheline and K-feldspar contain most of the K budget in BIP samples, we conclude that young ages reflect poor retention of ^{40}Ar by nepheline and/or K-feldspar. Excluding these young ages and considering only U-Pb zircon and $^{40}Ar/^{39}Ar$ amphibole and phlogopite ages yields new insights into the age of BIP activity. We conclude that the BIP was active at 83.5 ± 0.2 to 76.2 ± 0.6 Ma, an interval of about 7 m.yr. This is also consistent with the clear stratigraphic constraints at Pilot Knob (fig. 2, *43*), indicating that volcanism was contemporaneous with deposition of Santonian to Campanian strata (Burke et al. 1969), corresponding to an absolute age range of 89.3 ± 1 to 70.6 ± 0.6 Ma (Gradstein et al. 2005).

It appears that felsic BIP lithologies (phonolites and tephriphonolite) are not contemporaneous with the mafic lithologies. Our study indicates that the felsic lithologies range in age from 76.2 ± 0.6 to 78.8 ± 0.7 Ma, based on our best $^{40}Ar/^{39}Ar$ and U-Pb results from six different outcrops representing a time frame of approximately 2.6 m.yr., during which felsic activity occurred. Although we have only three results for mafic centers in the BIP, the best estimates of eruption ages are 81.5 ± 0.8 to 83.5 ± 0.2 Ma. Miggins et al. (2004) reported various eruption ages (not all t_p) for five mafic sample locations ranging from 78.5 ± 0.12 to 82.8 ± 0.13, although some of those results appear problematic. On the basis of our best results, two phases of BIP activity are apparent, earlier nephelinite- to

basanite-dominated activity at ~81.5–83.5 Ma and phonolite-dominated activity at ~76–79 Ma. A gap of as much as 2 m.yr. appears to separate the two phases, as indicated by the youngest mafic and the oldest felsic ages in the BIP. Field observations indicate that individual felsic and mafic centers are discrete bodies; no interfingering or crosscutting relationships between the two types have been documented. The time gap may potentially represent the time required for phonolites to evolve from a BIP mafic parent.

Significance of Xenocrystic Zircon. Several samples contained xenocrystic zircon that yielded much older ages for some grains compared with the majority of grains yielding Late Cretaceous ages. U-Pb concordia ages of the xenocrystic zircon range from 681 to 978 Ma, and $^{207}Pb/^{206}Pb$ ages range from 558 to 982 Ma (2σ; table 3). The significance of the xenocrystic zircons is that they indicate crustal contamination of melts ascending through the lithosphere, which picked up these zircons from crust or sediments during ascent. Xenocryst ages do not implicate Mesoproterozoic crust of the Texas part of the North American craton because this lacks Neoproterozoic-age zircons (Gleason et al. 2002, 2007). Neoproterozoic zircons derived from Gondwanaland are reported from metasediments incorporated in the Ouachita orogenic belt (Gleason et al. 2007) and are suspected to underlie the BIP, and we conclude that this is the principal source of BIP xenocrystic zircons.

Monogenetic versus Polygenetic Magmatism in the BIP. The BIP is an intraplate magmatic province, exploiting older lithospheric structures that have been reactivated in a net extensional stress regime, producing small-volume, low-degree melts enriched in alkali and volatile (especially CO_2) elements (Griffin 2008; Griffin et al. 2009). Comagmatic eruptions appear to have been facilitated by forces related to the Late Cretaceous Hidalgo orogeny in Mexico (Bird 2002). The cessation of BIP volcanism after a relatively short time, and hence its monogenetic character, is most likely related to one of the following three factors: (1) the exhaustion of alkali and volatile element budgets in the mantle had promoted small-degree melting, (2) the North American plate may have moved enough so that the lithospheric discontinuity lost communication with the enriched mantle domain where melting was occurring, or (3) the permissive stress regimes changed orientation enough to prevent ascent of later melts. Bird (2002) contends that σ_1 orientations had remained relatively constant at 68° (United States) and 75° (Mexico) between 85 and 50 Ma, suggesting that the cessation of magmatism was not related to the relaxation or change in orientation of stress regimes. Given plate motion rates of 2.0–2.6 cm/yr, at an orientation (based on inferred traces of the Bermuda hot spot track) of 280° (Morgan 1983) to 300° (Duncan 1984), the maximum displacement of the lithospheric discontinuity relative to the locus of melting is on the order of 68 km (between 81.5 and 84.1 Ma). Plotting these orientations on a map of the BIP, relative to our mafic rock ages in the western extreme of the province, and given the unrealistic criteria that the locus of melting must lie directly under a volcanic center, it is apparent that 68 km of plate motion would have resulted in the locus of melting having moved under an area with the most BIP volcanic centers. We suggest that the plate motion argument cannot explain the monogenetic nature of the BIP. Instead, the best explanation for the cessation of volcanism in the BIP is exhaustion of the alkali and volatile budgets within the zone of melting. The presence of alkali and volatiles (especially CO_2) in the mantle effectively lowers the temperature of melting (Griffin 2008; Griffin et al. 2009), so even though stress regimes may have remained favorable between 85 and 50 Ma, the exhaustion of alkali and volatile budgets in the mantle effectively shut off further melting. If the BIP were to have been a polygenetic complex, it would have required periodic replenishment of alkali and volatile elements into the zone of melting.

Bailey and Woolley (2005) related similar factors to polygenetic alkaline magmatism in Africa over the past 180 m.yr., contending that alkaline magmatism is common on continental plates, asserting that lithospheric thickness and geothermal gradients exert major influences on where and when volcanism begins, and recognizing that reactivation of older lithospheric structures is strongly correlated with the initiation of magmatism. Polygenetic centers may form over long periods by repeated reactivation of preexisting lithospheric structures. Continued plate motion may bring new (alkali- and volatile-enriched?) asthenospheric domains within the realm of preexisting lithospheric structures (Bailey and Woolley 2005). Because small-degree melts enriched in alkali and volatile elements are commonly associated with alkalic magmatic complexes, volatile replenishment must occur in order for new melting events to occur (Bailey and Woolley 2005). Given the common traits of each style of magmatism, the differences (and duration) between monogenetic and polygenetic fields appear to be controlled by the amount of alkali- and

volatile-enriched mantle available for melting, the timing required for replenishment of the alkali and volatile elements, and the maintenance or reactivation of net extensional stresses along a preexisting lithospheric discontinuity. Periodic replenishment and reactivation of lithospheric discontinuities alone are insufficient to initiate melting; both events must occur in order to induce subsequent magmatic events.

Implications for a Mantle Plume–Hot Spot Track Origin of the BIP. Temporal relations of magmatic zones are used to test mantle plume theory, which suggests that for lithosphere overriding a fixed mantle plume, a hot spot track develops, recording an age-progressive magmatic belt that youngs in the direction opposite that of the plate motion (Morgan 1971; Campbell 2001, 2005). Cox and Van Arsdale (2002) suggested that the igneous centers in southwest Arkansas, the Monroe uplift, and the Jackson Dome (fig. 1) may be the result the North American continent overriding a mantle plume, using the projected Great Meteor plume track (~120° trend) of Duncan (1984) as evidence. The Great Meteor track was no closer to the BIP than 700 km at its closest approach at the eastern end of the BIP. There does not appear to be an age progression of centers within the BIP. We have demonstrated by isotopic means that volcanism was concentrated into two discrete 2.6-m.yr. episodes, one mafic and one felsic. The spatial intermingling of mafic and felsic centers differing in age by a minimum of 2.8 m.yr. does not provide evidence for a time-progressive track. Although the easternmost igneous center (Pilot Knob; fig. 2, *43*) of the BIP is not isotopically as well constrained as some other centers, stratigraphic relations there support contemporaneous eruption with the mafic episode in the western portions of the BIP. We therefore reject the mantle plume model as a potential emplacement mechanism and argue that the preferred model of reactivation of older lithospheric structures promoting low-degree melting of volatile (especially CO_2) charged asthenosphere provides the best model to explain the occurrence of the BIP.

Conclusions

Late Cretaceous volcanism in the BIP, characterized by the group 1 nephelinite association of Le Bas (1978, 1987), formed a small-volume system of intrusive and extrusive igneous bodies along the trend of the Pennsylvanian Ouachita orogenic belt in central Texas. This also marks a discontinuity between Grenville-age cratonic lithosphere to the north and west and Jurassic-age transitional lithosphere to the south and east. New high-resolution $^{40}Ar/^{39}Ar$ mineral separate and U-Pb zircon ages provide additional insights into the timing of BIP magmatism. Our study demonstrates that previous $^{40}Ar/^{40}K$ ages (Burke et al. 1969; Baldwin and Adams 1971) are as much 17% too young and that even modern $^{40}Ar/^{39}Ar$ techniques applied to nepheline-K-feldspar or groundmass concentrates give unreliable $^{40}Ar/^{39}Ar$ ages. Such young ages reflect the fact that most K in the BIP samples is concentrated in K-feldspar and nepheline, which have poor retention of radiogenic ^{40}Ar. Significantly older and similar ages in our study were obtained by U-Pb zircon and $^{40}Ar/^{39}Ar$ amphibole and phlogopite techniques, and we conclude that these provide the most reliable indication of when BIP igneous activity occurred.

Magmatism occurred in two discrete phases, each associated with distinct petrological characteristics. Mafic lavas, comprising melilite olivine nephelinites, olivine nephelinites, basanites, and alkali basalts, erupted at 81.5–84.1 Ma, a period of only 2.6 m.yr. Felsic magmatism, comprising phonolites, tephriphonolite, and phonotephrites, occurred at 76.2–78.8 Ma, a range of just 2.6 m.yr. The relatively short time of volcanism is consistent with results for other group 1 nephelinite complexes on Earth. The monogenetic nature of the BIP was most likely a result of exhaustion of alkali and volatile elements in the zone of melting.

ACKNOWLEDGMENTS

We wish to acknowledge the efforts of F. A. Hubacher and J. S. Linder at the Radiogenic Isotopes Laboratory, Ohio State University, and J. Wooden, F. Mazdab, and staff at the SUMAC facility. Discussions with D. Barker and T. Ewing were helpful during the initial stages of the project. This work was supported by the University of Texas at Dallas, the Dallas Geological Society, and the Gulf Coast Association of Geological Societies through scholarship funding to W. R. Griffin and through a Graduate Research Grant from the Geological Society of America to W. R. Griffin. Additional funding for this project was provided by the National Science Foundation (grant 0224551 to M. I. Leybourne; grants EAR-0107054 and EAR-0137546 to K. A. Foland).

REFERENCES CITED

Bailey, D. K., and Woolley, A. R. 2005. Repeated, synchronous magmatism within Africa, timing, magnetic reversals, and global tectonics. *In* Folger, G. R.; Natland, J. H.; Presnall, D. C.; and Anderson, D. L., eds. Plates, plumes, and paradigms. Geol. Soc. Am. Spec. Pap. 388:365–378.

Baksi, A. K. 1997. The timing of Late Cretaceous alkalic igneous activity in the northern Gulf of Mexico basin, southeastern USA. J. Geol. 105:629–643.

Baldwin, O. D., and Adams, J. A. S. 1971. $^{40}K/^{40}Ar$ ages of the alkalic igneous rocks of the Balcones fault trend of Texas. Tex. J. Sci. 22:223–231.

Barker, D. S. 1996. Nephelinite-phonolite volcanism. *In* Mitchell, R. H., ed. Undersaturated alkaline rocks: mineralogy, petrogenesis, and economic potential. Mineral. Assoc. Can. Short Course Ser. 24:23–44.

Barker, D. S., and Young, K. P. 1979. A marine Cretaceous nepheline basanite volcano at Austin, Texas. Tex. J. Sci. 31:5–24.

Bird, P. 2002. Stress direction history of the western United States and Mexico since 85 Ma. Tectonics 21: 1–12.

Black, L. P.; Kamo, S. L.; Allen, C. M.; Davis, D. W.; Aleinikoff, J. N.; Valley, J. W.; Mundil, R.; et al. 2004. Improved $^{206}Pb/^{238}Pb$ microprobe geochronology by the monitoring of a trace-element-related matrix effect: SHRIMP, ID-TIMS, ELA-ICP-MS and oxygen isotope documentation for a series of zircon standards. Chem. Geol. 205:115–140.

Burke, W. H.; Otto, J. B.; and Denison, R. E. 1969. Potassium-argon dating of basaltic rocks. J. Geophys. Res. 74:1082–1086.

Byerly, G. R. 1991. Nature of igneous activity. *In* Salvador, A., ed. The Gulf of Mexico basin (Geology of North America, Vol. J). Boulder, CO, Geol. Soc. Am., p. 91–108.

Campbell, I. 2001. Identification of ancient mantle plumes. *In* Ernst, R. E., and Buchan, K. L., eds. Mantle plumes: their identification through time. Geol. Soc. Am. Spec. Pap. 352:5–21.

———. 2005. Large igneous provinces and the mantle plume hypothesis. Elements 1:265–269.

Cook, C.; Briggs, R. M.; Smith, I. E. M.; and Maas, R. 2005. Petrology and geochemistry of intraplate basalts in the South Auckland volcanic field, New Zealand: evidence for two coeval magma suites from distinct sources. J. Petrol. 46:473–503.

Corti, G.; van Wijk, J. W.; and Bonini, M. 2003. Transition from continental break-up to puctiform seafloor spreading: how fast, symmetric and magmatic. Geophys. Res. Lett. 30:8046–8049.

Cox, R. T., and Van Arsdale, R. B. 2002. The Mississippi embayment, North America: a first-order continental structure generated by the Cretaceous superplume mantle event. J. Geodynam. 34:163–176.

Dalrymple, G. B. 1979. Critical tables for conversion of K-Ar ages from old to new constants. Geology 7:558–560.

Duncan, R. A. 1984. Age progressive volcanism in the New England seamounts and the opening of the central Atlantic Ocean. J. Geophys. Res. 89:9980–9990.

Edwards, B. R., and Russell, J. K. 1999. Northern Cordilleran volcanic province: a northern basin and range? Geology 27:243–246.

———. 2000. Distribution, nature and origin of Neogene-Quaternary magmatism in the northern Cordilleran volcanic province, Canada. Geol. Soc. Am. Bull. 112: 1280–1295.

Ewing, T. E., and Caren, C. S. 1982. Late Cretaceous volcanism in south and central Texas: stratigraphic, structural and seismic models. Gulf Coast Assoc. Geol. Soc. Trans. 32:137–145.

Fitton. J. G. 1987. The Cameroon line, West Africa: a comparison between oceanic and continental alkaline volcanism. Geol. Soc. Lond. Spec. Publ. 30:273–291.

Foland, K. A.; Fleming, T. H.; Heimann, A.; and Elliot, D. H. 1993. Potassium-argon dating of fine-grained basalts with massive Ar loss: application of the $^{40}Ar/^{39}Ar$ technique to plagioclase and glass from the Kirkpatrick basalt, Antarctica. Chem. Geol. 107:173–190.

Galloway, W. E.; Bedout, D. G.; Fisher, W. L.; Dunlap, W. L., Jr.; Cabrera-Castro, R.; Lugo-Rivera, J. E.; and Scott, T. M. 1991. Cenozoic. *In* Salvador, A., ed. The Gulf of Mexico basin (Geology of North America, Vol. J). Boulder, CO, Geol. Soc. Am., p. 245–324.

Gleason, J. D.; Finney, S. C.; and Gehrels, G. E. 2002. Paleotectonic implications of a mid- to late-Ordovician provenance shift, as recorded in sedimentary strata of the Ouachita and southern Appalachian Mountains. J. Geol. 110:291–301.

Gleason, J. D.; Gehrels, G. E.; Dickinson, W. R.; Patchett, P. J.; and Kring, D. A. 2007. Laurentian sources for detrital zircon grains in turbidite and deltaic sandstones of the Pennsylvanian Haymond Formation, Marathon assemblage, west Texas, USA. J. Sediment. Res. 77:888–900.

Gourgaud, A., and Vincent, P. M. 2004. Petrology of two continental alkaline intraplate series at Emi Koussi volcano, Tibesti, Chad. J. Volcanol. Geotherm. Res. 129:261–290.

Gradstein, F. M.; Ogg, J. G.; and Smith, A. G. 2005. A geologic time scale 2004. Cambridge University Press, Cambridge.

Griffin, W. R. 2008. Geochemistry and geochronology of the Balcones igneous province, Texas. PhD dissertation, University of Texas, Dallas.

Griffin, W. R.; Stern, R. J.; and Leybourne, M. I. 2009. Episodic Late Cretaceous volcanism in the Balcones igneous province, Texas. Geol. Soc. Am. Abstr. Program 141:14.

Ireland, T. T., and Williams, I. S. 2003. Considerations

in zircon geochronology by SIMS. Rev. Mineral. Geochem. 53:215–241.
Johansen, T. S.; Hauff, F.; Hoernle, K.; Klügel, A.; and Kokfelt, T. F. 2005. Basanite to phonolite differentiation within 1550–1750 yr: U-Th-Ra isotopic evidence from A. D. 1585 eruption on La Palma, Canary Islands. Geology 33:897–900.
Kay, R. W., and Kay, S. M. 1993. Delamination and delamination magmatism. Tectonophysics 219:177–189.
King, S. D., and Anderson, D. L. 1998. Edge-driven convection. Earth Planet. Sci. Lett. 160:289–296.
Lanphere, M. A. 1999. Comparison of conventional K-Ar and $^{40}Ar/^{39}Ar$ dating of young mafic volcanic rocks. Quat. Res. 53:294–301.
Le Bas, M. J. 1978. Nephelinite volcanism at plate interiors. Bull. Volcanol. 41:459–462.
———. 1987. Nephelinites and carbonatites. *In* Fitton, J. G., and Upton, B. G. J., eds. Alkaline igneous rocks. Geol. Soc. Lond. Spec. Publ. 30:53–84.
Liégeois, J. P.; Benhallou, A.; Azzouni-Sekkal, A.; Yahiaoui, R.; and Bonin, B. 2005. The Hoggar swell and volcanism: reactivation of the Precambrian Tuareg shield during Alpine convergence and West African Cenozoic volcanism. *In* Folger, G. R.; Natland, J. H.; Presnall, D. C.; and Anderson, D. L., eds. Plates, plumes and paradigms. Geol. Soc. Am. Spec. Pap. 338: 379–400.
Ludwig, K. R. 2001. 2001 Squid 1.02 add-on for Excel. Berkeley Geochronology Center Special Publication 2. Berkeley, Berkeley Geochronology Center.
Matthews, T. F. 1986. The petroleum potential of "serpentine plugs" and associated rocks, central and south Texas. Baylor Geol. Stud. Bull. 44:1–43.
Merrill, R. K. 1983. Source of the volcanic precursor to Upper Cretaceous bentonite in Monroe County, Mississippi. Miss. Geol. 3:1–6.
Miggins, D. P.; Blome, C. D.; and Smith, D. V. 2004. Preliminary $^{40}Ar/^{39}Ar$ geochronology of igneous intrusions from Uvalde County, Texas: defining a more precise eruption history for the southern Balcones volcanic province. U.S. Geol. Surv. Open File Rep. 2004-1031:33.
Mitchell, R. H., and Platt, R. G. 1983. Primitive nephelinitic volcanism associated with rifting and uplift in the Canadian Arctic. Nature 303:609–612.
Morgan, W. J. 1971. Convection plumes in the lower mantle. Nature 230:42–43.
———. 1983. Hot spot tracks and the early rifting of the Atlantic. Tectonophysics 94:123–139.
Ngounouno, I.; Déruelle, B.; and Demaiffe, D. 2000. Petrology of the bimodal Cenozoic volcanism of the Kapsiki plateau (northernmost Cameroon), central Africa. J. Volcanol. Geotherm. Res. 102:21–44.
Nielsen, T. F. D. 1981. The ultramafic cumulate series, Gardiner Complex, East Greenland: cumulates in a shallow-level magma chamber of a nephelinitic volcano. Contrib. Mineral. Petrol. 76:60–72.
Sawyer, D. S.; Buffler, R. T.; and Pilger, R. H., Jr. 1991. The crust under the Gulf of Mexico Basin. *In* Salvador, A., ed. The Gulf of Mexico basin (Geology of North America, Vol. J). Boulder, CO, Geol. Soc. Am., p. 53–72.
Stacey, J. S., and Kramers, J. D. 1975. A proximation of terrestrial lead isotope evolution by a two-stage model. Earth Planet. Sci. Lett. 26:207–221.
Strong, W. M. 1957. Structural geology of Pilot Knob area, Travis County, Texas. MA thesis, University of Texas, Austin.
Ulrych, J.; Cajz, V.; Pivec, E.; Novák, J. K.; and Nekovarík, C. 2000. Cenozoic intraplate alkaline volcanism of western Bohemia. Stud. Geophys. Geodyn. 44:346–351.
Williams, I. S. 1997. U-Th-Pb geochronology by ion microprobe: not just ages but histories. Soc. Econ. Geol. Rev. Econ. Geol. 7:1–35.
Yongtao, F., and Anchun, L. 2003. Petrology, geochemistry, and Nd-Sr-Pb isotopic properties of volcanic rocks in Daheishan Island, Panglai, Shandong Province. Mar. Sci. Bull. 5:29–39.
Young, K.; Caran, S. C.; and Ewing, T. E. 1982. Cretaceous volcanism in the Austin area, Texas. Austin Geol. Soc. Guidebook 4, 66 p.
Zartman, R. E. 1977. Geochronology of some alkalic rock provinces in eastern and central United States. Annu. Rev. Earth Planet. Sci. 5:257–286.